UCRL-LR-148382
Thesis

A Programmable MicroFluidic Processor: Integrated and Hybrid Solutions

K. A. Rose
Master of Science

May 10, 2002

U.S. Department of Energy
Lawrence Livermore National Laboratory

DISCLAIMER

This work was performed under the auspices of the U. S. Department of Energy by the University of California, Lawrence Livermore National Laboratory under Contract No. W-7405-Eng-48.

A Programmable MicroFluidic Processor: Integrated and Hybrid Solutions

by

Klint A Rose

B.S. Mechanical Engineering
Massachusetts Institute of Technology, 2001

SUBMITTED TO THE DEPARTMENT OF MECHANICAL ENGINEERING IN PARTIAL FULFILLMENT OF THE REQUIREMENTS FOR THE DEGREE OF

MASTER OF SCIENCE IN MECHANICAL ENGINEERING
AT THE
MASSACHUSETTS INSTITUTE OF TECHNOLOGY

JUNE 2002

Signature of Author: _____
Department of Mechanical Engineering
May 10, 2002

Certified by: _____
Douglas P. Hart
Associate Professor of Mechanical Engineering
Thesis Supervisor

Accepted by: _____
Professor Ain A. Sonin
Professor of Mechanical Engineering
Chairman, Committee for Graduate Students

A Programmable MicroFluidic Processor: Integrated and Hybrid Solutions

by

Klint A Rose

Submitted to the Department of Mechanical Engineering
on May 10, 2002 in Partial Fulfillment of the
Requirements for the Degree of Master of Science in
Mechanical Engineering

ABSTRACT

The Programmable Fluidic Processor (PFP), a device conceived of by researchers at MD Anderson Cancer Center, is a reconfigurable and programmable bio-chemical analysis system designed for handheld operation in a variety of applications. Unlike most microfluidic systems which utilize channels to control fluids, the PFP device is a droplet-based system. The device is based on dielectrophoresis; a fluid transport phenomenon that utilizes mismatched polarizability between a droplet and its medium to induce droplet mobility. In the device, sample carrying droplets are polarized by an array of electrodes, individually addressable by subsurface microelectronics. My research focused on the development of a polymer-based microfluidic injection system for injecting these droplets onto the electrode array.

The first of two device generations fabricated at LLNL was designed using extensive research and modeling performed by MD Anderson and Coventor. Fabricating the first generation required several iterations and design changes in order to generate an acceptable device for testing. Difficulties in planar fabrication of the fluidic system and a narrow channel design necessitated these changes. The second generation device incorporated modifications of the previous generation and improved on deficiencies discovered during experimentation with the initial device. Extensive modeling of the injection channels and fluid storage chamber also aided in re-designing the device's microfluidic system. A micromolding technique with interlocking features enabled precise alignments and dimensional control, critical requirements for device optimization. Fabrication of a final device will be fully integrated with the polymer-based microfluidics bonded directly to the silicon-based microelectronics. The optimized design and process flow developed in the trial generations will readily transfer to this approach.

Thesis Supervisor: Douglas P. Hart
Title: Associate Professor of Mechanical Engineering

Table of Contents

List of Figures

1 Introduction

The Programmable Fluidic Processor (PFP) is a general-purpose analysis system designed to provide re-programmable and adaptive analysis for a variety of applications from industrial monitoring to biological warfare detection. Researchers at the MD Anderson Cancer Center conceived of the PFP concept and performed initial proof-of principle experimentation for the device [1]. Development of a compact microfabricated device is a collaborative effort between MD Anderson and the Lawrence Livermore National Laboratory Center for Microtechnology, with assistance from University of California at Davis, Coventor, and Lynntech Inc. The project is funded through the Defense Advanced Research Project Agency Biological Fluidic Chips program.

The DARPA BioFLIPS program was established to "demonstrate technologies for microprocessors capable of on-chip reconfiguration and self-calibration via feedback control. The prototypes developed in this program will be capable of on-chip sample-to-answer biological fluid assays, and will form the basis for the future goal of real-time, unobtrusive monitoring and control of a person's health parameters [2]." Through integration of microfluidics, high-voltage integrated circuitry, and controlled dielectrophoresis, the final version of the Programmable Fluidic Processor will meet the objectives of the BioFLIPS program.

The PFP device is unique from most microfluidic analysis systems because the assay is performed on droplets in a chamber versus fluids in microchannels. The network of channels in a conventional fluidic system greatly constrains the functions that can be

The system overview for the PFP device is shown in Figure 1.1. Pico- to nanoliter fluid droplets containing test samples are injected from a storage chamber into the PFP chamber. Using multiple storage chambers and injectors, several different fluids can be injected simultaneously into the chamber allowing for numerous microchemistry interactions between droplets. The surface of the PFP chamber contains an extensive array of evenly spaced electrodes. Underlying high voltage integrated circuitry controls the potential at each individual electrode and enables the use of dielectrophoresis to arbitrarily move droplets along the surface in a programmed sequence. The PFP device is then integrated with system wide electronics and software and packaged into a handheld device for use in an extensive range of field applications. The fields in which the device could be used include: medicine, environmental, industrial monitoring, pharmaceutical and biological warfare detection. The ability to modify the working solutions and to meter these solutions and their interactions provides numerous applications for the devices use.

As diagrammed in Figure 1.2, the development plan for the PFP device consisted of a three generational progression of microfabricated devices. The first generation electronics and microfluidics were fabricated and tested individually rather than together in a device. The second generation was developed as a hybrid device, with the control electronics eventually connected to the microfluidics in an off-chip arrangement. The final device will be an integrated device, designed based on the knowledge gained from the previous generations.

fabrication and a channel design for the fluidic system that was not feasible. The difficulties in fabrication arose due to stringent alignment constraints necessary in the device that were difficult to achieve through standard planar microfabrication. After fabricating first generation devices, I developed models of the microfluidic system to optimize the design and refined the process flow to ease in fabrication. The second generation utilized these and other modifications to improve on deficiencies in the device. Among these improvements was an alignment procedure to precisely place the fluidic system with respect to the device substrate and a tapered channel design to eliminate clogging problems discovered in the first generation. The design and process flow for the second generation will be slightly modified to create an integrated final device with the microfluidic system bonded directly onto the microelectronics chip.

voltage integrated circuits, and it mandated the use of a suitable "mock" substrate for experimental fabrication. The flexibility afforded by polymer fabrication methods made this material and its associated processes the most appropriate choice for fluid elements on the patterned wafer. Glass was determined to be the best-suited substrate for test generations due to its similarities with the exposed silicon dioxide layer that will eventually insulate the finished microelectronics. Lastly, the electrode dimensions determined through modeling and experimentation determined the space requirements for the electronics which in turn determined the necessary size for the PFP chamber.

2.2 Polymer Fabrication

The PFP fluid storage and injection system was designed and fabricated by the LLNL Microtechnology Center, with considerable input from the overall project team. The device employs and expands upon previous polymer techniques to fabricate a channel-less and reconfigurable system for performing biochemical assays. The Microtechnology Center has used polymers to fabricate multiple microfluidic devices, and the PFP device is a logical extension of these capabilities.

Professor George Whiteside's group at Harvard established the foundation for these polymer techniques [3]. The group developed what is termed "Soft Lithography," a micromolding fabrication technique that utilizes the properties of the silicone rubber poly(dimethylsiloxane), or PDMS. As shown in Figure 2.3 below, the process begins with mold masters that are patterned via photolithography to develop raised features on the surface of the mold substrate. The PDMS (Sylgard 184, Dow Corning) is a 10:1 mass ratio of liquid precursor and curing agent. Once mixed and thoroughly degassed, the

polymer offers a tremendous adaptability in using the material. The PDMS is also hydrophobic, an important feature for controlling flow through the microchannels and developing droplets in the PFP chamber.

2.3 Dielectrophoresis

The dielectrophoresis concept used for droplet mobility is made possible through MD Anderson Cancer Center's extensive research on the subject. Dielectrophoresis (DEP) is the movement of an object by a spatially non-uniform electrical field. The phenomenon only arises when the object has a different electrical polarizability relative to its surroundings. Dielectrophoresis is distinct from the well-known electrophoresis because it is not affected by any net charge on the object, an advantageous characteristic when performing assays with highly charged biomolecules.

Positive or negative DEP can be encountered, depending on the relative polarizability of the object and it's surrounding. Positive DEP occurs when the object is more polarizable than its surroundings, causing it to be pulled towards higher field regions. Negative DEP is the reverse case, in which the object is less polarizable than its surrounding and is therefore pushed away from the higher field regions. Positive and negative DEP forces can be produced from an AC electric field with frequencies in the range of 10 kHz to 1 MHz, a range that avoids bubble formation and other disruptive effects from the onset of electrolysis. Surface electrodes can be used to generate the necessary fields, and mobility of particles is achieved by varying the field between adjacent electrodes. Using this strategy, droplets in the PFP device can be moved along an electrode array to perform a variety of assays through mixing of various fluids. Due to

surface tension in the droplet, this mixing occurs when two droplets are brought into contact with one another. DEP offers sufficient control to selectively manipulate droplets within their carrier medium or hold them in place while a new medium is washed over them [4].

The MD Anderson team has also developed models to describe the forces generated by DEP fields. The following equation uses Green's theorem to describe the DEP force on a particle due to an imposed electric field [5].

$$\left\langle \vec{F}(t) \right\rangle = 2\pi\varepsilon_m r^3 \left(\mathrm{Re}(f_{CM}(\omega))\nabla E(rms)^2 + \mathrm{Im}(f_{CM}(\omega))(E_{x0}^2\nabla\varphi_x + E_{y0}^2\nabla\varphi_y + E_{z0}^2\nabla\varphi_z \right) \quad (1)$$

$$f_{CM}(\varepsilon_p^*, \varepsilon_m^*, \omega) = \frac{\varepsilon_p^*(\omega) - \varepsilon_m^*(\omega)}{\varepsilon_p^*(\omega) + 2\varepsilon_m^*(\omega)} \quad (2)$$

Equation (2), also from reference [5], is the Clausius-Mossotti factor that embodies the frequency-dependent dielectric properties $\varepsilon_p^*(\omega)$ and $\varepsilon_m^*(\omega)$ of the particle and its suspending medium, respectively. E(rms) is the root mean square value of the applied electric field, and angular frequency is denoted by ω. E_{i0} and j_i (where i=x; y; z) are the magnitudes and phases, respectively, of the field components in the principal axis directions. This first order model is sufficient for analysis in the PFP device although MD Anderson has derived a more general expression to account for induced higher order poles [6].

Examination of the equation reveals two independent force contributions: a field inhomogeneity component and a traveling field component. Droplets are pushed towards strong or weak field regions depending on the induced dipole moment in the particle and the spatial non-uniformity of the field magnitude. This force is described by the real component in equation 1, referred to as the field inhomogeneity component. In the PFP

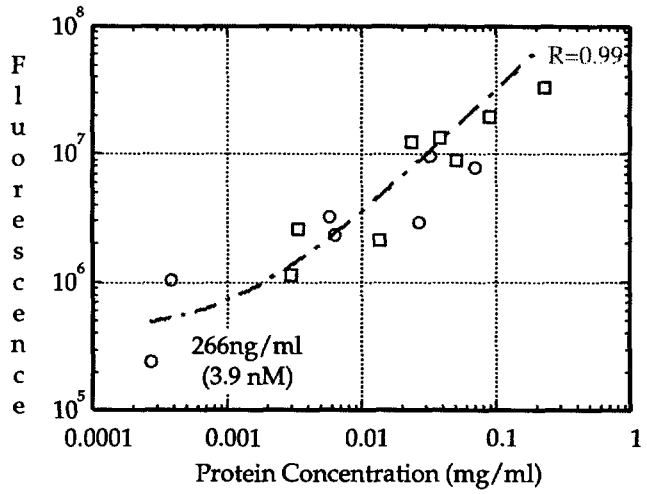

Figure 2.6: Log-log plot of fluorescence vs. BSA concentration in the droplets. This equation relating these values can be used to determine BSA concentration based on fluorescence in a detection system [1].

This experiment proves that the PFP device can be an effective detection system using the principle of dielectrophoresis to combine various chemicals on the surface to perform numerous assays. By adding programmability of the electrodes as well as a microfluidic system for injection and removal of chemicals, the final PFP device promises to provide an adaptive analysis tool for a large range of field applications.

3 First Generation Design

The critical task in the preliminary design of a PFP device was determining appropriate materials and processes that could eventually be used in an integrated device. Material requirements ranged from a hydrophobic surface in the PFP chamber for maintaining spherical droplets to compatibility issues between the microfluidic and microelectronic materials. A passivation layer was also necessary between droplets in solution and the metal electrodes to avoid shorting the electronics. Electrode size and spacing as well as injection channel size were important design aspects that affected the fabrication processes pursued. For the first generation, the high voltage integrated circuitry that would eventually control the dielectrophoresis in the chips and the droplet forming microfluidics were designed completely separately to expedite their progress toward a hybrid device in the second generation.

Because the final device was intended to be an integrated device with the microfluidics fabricated directly onto the integrated circuits, design decisions in the initial stage had to facilitate this combination. Glass was therefore chosen as the substrate for the first generation because its properties are very similar to those of SiO_2, the typical insulation layer used over microelectronics. The optical transparency of glass and fabrication capabilities at LLNL Microtechnology Center also made the material the most appropriate choice. Direct integration of microelectronics with micro- and meso-scale fluidics is a novel approach that demanded a fabrication process to which the underlying

performed. Even microfluidic devices with three-dimensional channels and vias have limited capabilities. The primary advantage gained using a droplet-based system is ability to reprogram the device to perform a new assay whereas a channel system typically requires a completely new design and device. The picoliter to microliter size droplets used in the system are also advantageous as they insure accurate metering of samples and reagents, correlating to more precise results during testing. Continuous flow of sample fluids, with periodic micro-sampling of the fresh samples, can be conducted without the need to pressurize or pump the fluids. This also eliminates the accumulation of stale, unused samples in the channels leading to injectors.

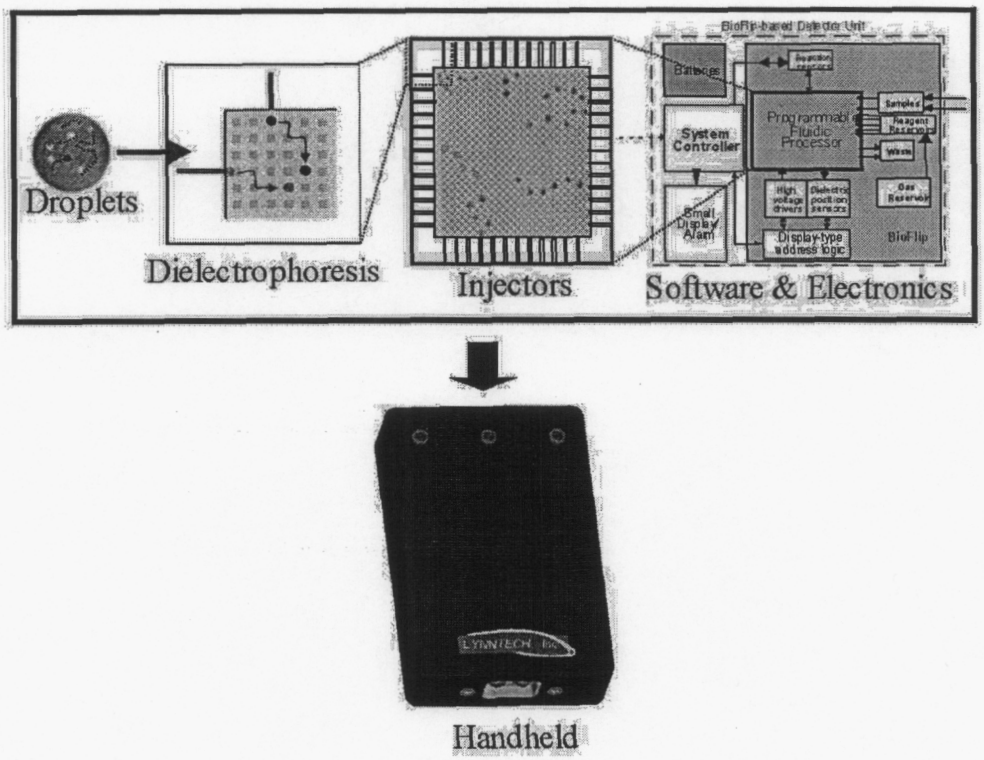

Figure 1.1: System expansion of the PFP device. Droplets of solution are injected onto a set of electrodes to perform dielectrophoresis. The electrodes are controlled by integrated circuits and other electronics.

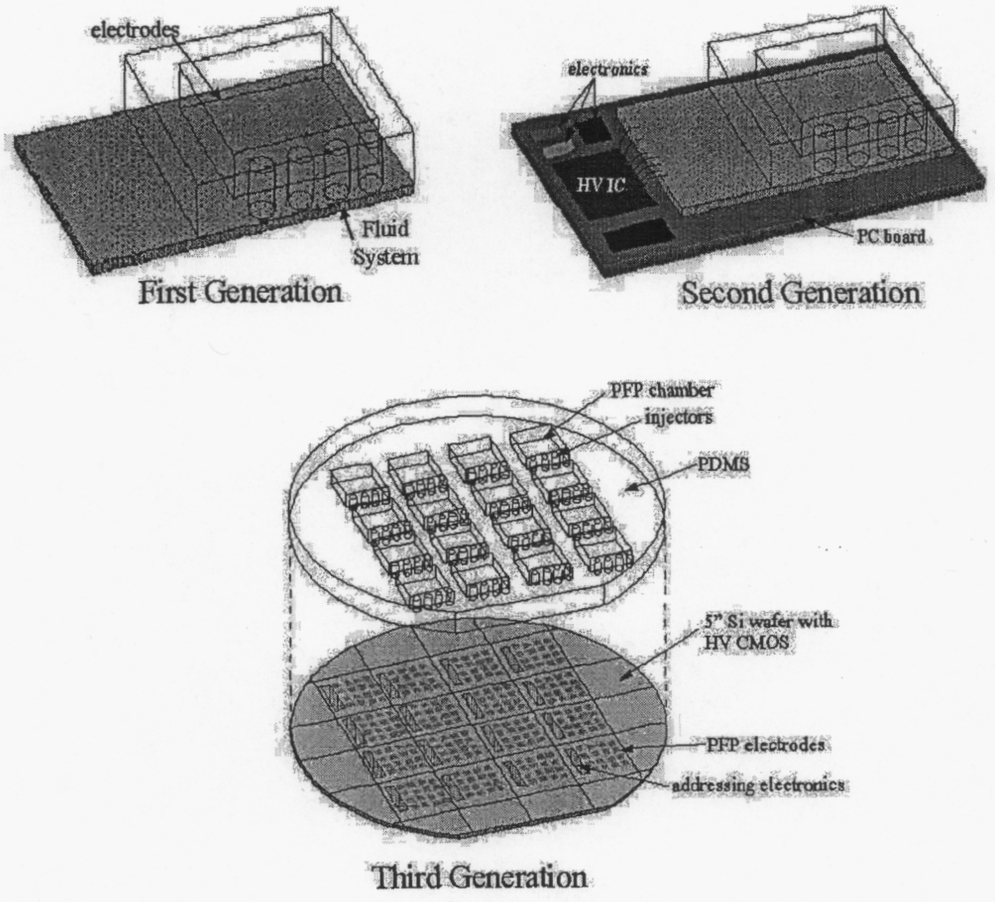

Figure 1.2: First generation device for testing design and fabrication of microfluidic system. Second Generation hybrid device with microfliudics and microelectronics connected via a PC board. Integrated third generation device with microfluidics bonded directly to the electronics.

My research at the LLNL Microtechnology Center was primarily focused on design and fabrication of the first and second generation devices. The first generation microfluidic system design was established using MD Anderson's extensive knowledge of dielectrophoresis and microfabrication experience from the LLNL Microtechnology Center. The fabrication, performed at LLNL, required several iterations and design changes in order to generate an acceptable device for testing. The completed device failed to meet many of the original design specifications due to difficulties during

2 Background

The PFP device consists of three major technologies including: fluidic storage and injection at the micro scale, fluid mobility with dielectrophoresis, and high voltage integrated circuits to drive the fluid movements. Figure 2.1 below diagrams the PFP concept. The magnified view on the left depicts an individual electrode with the addressing microelectronics and drivers. The magnified view on the right depicts the microfluidic features including the storage chamber, injection channel, and the PFP chamber where droplets are moved with dielectrophoresis. The successful production of a PFP device depended on the development of each of these features as well as their integration at the device level.

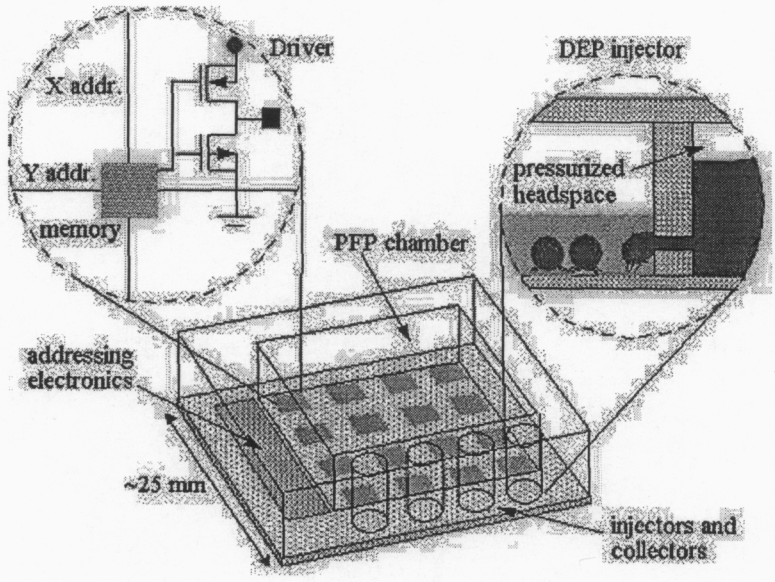

Figure 2.1: Model of the PFP device concept. The expanded view on the left depicts the integrated circuitry controlling each individual electrode. The view on the right is a simple model of the fluid being injected in droplet form onto the electrodes.

2.1 High Voltage Integrated Circuits

The high voltage integrated circuits used to control the dielectrophoresis electrodes were designed by Chuck McConaghy LLNL's Microtechnology Center and Professor Wayne Current of UC Davis. They created driver circuitry beneath each electrode to individually address the respective electrode. Design of these space-sensitive circuits was challenging because of the large transistor size necessary for high voltage logic. An illustration of the circuitry and electrode positioning is shown below in Figure 2.2. Due to this compact design, the electronics are scalable to any shape and size of array that might be necessary in the device.

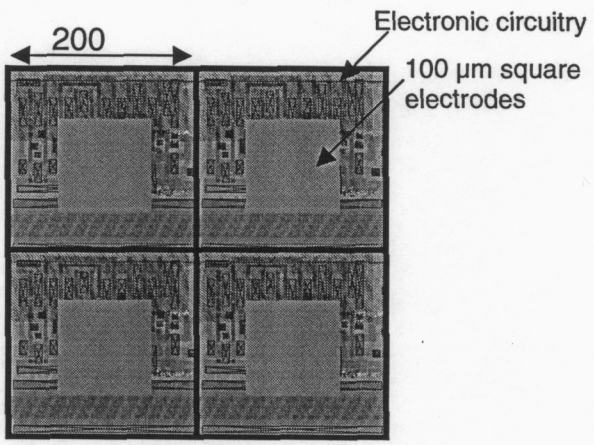

Figure 2.2: Representation of the electrodes and the circuitry beneath them.

Although the work involving the integrated circuit design and testing was integral to the project's success, it only affected the research described in this thesis by establishing material and dimensional requirements for the PFP chamber. The final generation device will be completely integrated with the microfluidics bonded directly on top of the microelectronics. This decision to integrate the two domains demanded a novel approach for post-processing the fluidic features onto a wafer containing the high

liquid polymer is poured onto the mold and cured under variable temperature conditions. The cured PMDS is then removed from the mold, resulting in microchannel imprints in the polymer surface.

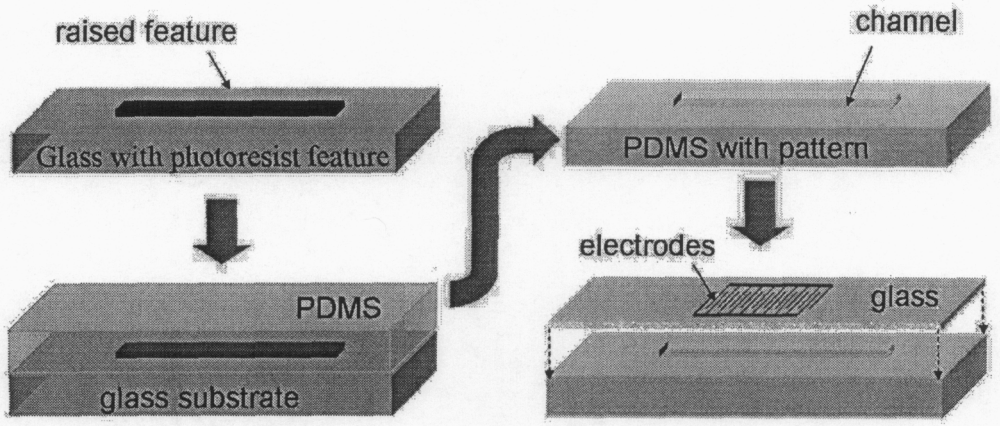

Figure 2.3: Soft Lithography process as developed by the Whitesides group. Photoresist is patterned on the glass or silicon surface in the desired shape of the channel. PDMS is poured onto the mold and cured. Once removed from the mold, an imprint of the resist creates a channel in the PMDS. A simple bonding procedure is used to seal the channel to PDMS, glass, or silicon.

Bonding the PDMS to a separate PDMS, glass, or silicon backing material seals the molded microchannels. This covalent bond is accomplished by removing all contaminants from the surfaces of both materials with an ethanol rinse then oxidizing the bonding surfaces in an RF facilitated oxygen plasma to activate their surface chemistry as described in [3]. The two materials can then be placed in conformal contact to create an instantaneous bond as the air is removed from the interface. This sealing process generates an irreversible bond with strength greater than that of the bulk material.

These basic processing principles were incorporated into the process flow of the PFP device with various modifications when necessary. The liquid state of PDMS allows it to be spun onto a substrate or cast in a mold and the flexible nature of the cured

device, this force allows droplets to be attracted or repelled from electrode edges. Droplets can be moved in parallel with the electric field due to the traveling field force which depends on the imaginary component of the induced dipole moment and the spatial non-uniformity of the field phase. Although these force components act independently they can be applied simultaneously to maintain a cell's vertical distance from an electrode while moving it in the horizontal plane. For the PFP application, only the vertical force from the field inhomogeneity is utilized.

Prior to LLNL Microtechnology fabricating a PFP device, MD Anderson used a basic experimental setup to assess the movement of droplets and determine whether assays could be preformed on the electrode arrays [1]. As proof-of-principle, an experiment was performed using an array of sixty-four gold electrodes patterned onto a glass substrate. As shown in the left picture of Figure 2.4 below, nine 65 nL droplets of o-pthalaldehyde, a fluorescence detectable chemical, were formed on the surface and held in place on individual electrodes with DEP forces.

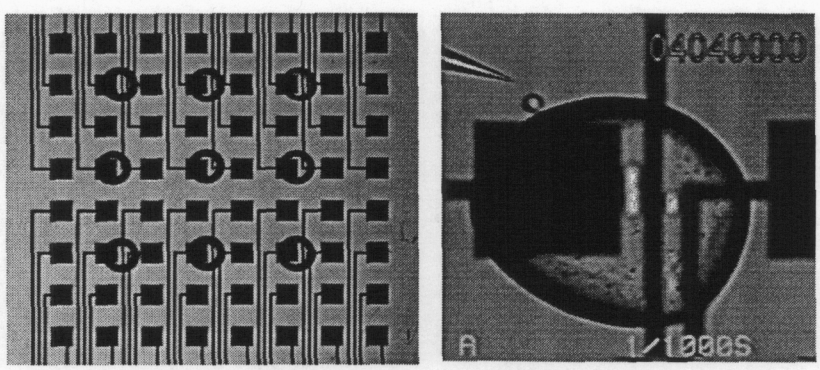

Figure 2.4: MD Anderson droplet experiments. Left: O-pthalaldehyde on an array of DEP controlled electrodes. Right: An individual droplet of bovine serum albumin is pulled from a micropipette into the larger droplet using DEP force [1].

Each of these o-pthalaldehyde droplets were then injected with 42 pl droplets of 5 mg/ml the protein bovine serum albumin (BSA). The droplets were pulled from the micropipette using an increased DEP force to attract the fluid. This effect was captured in the right picture of Figure 2.4. In this manner, a different number of droplets were injected into each of the nine OPA droplets. The fluorescence of the droplet array was then measured to determine the correlation between fluorescence and protein concentration.

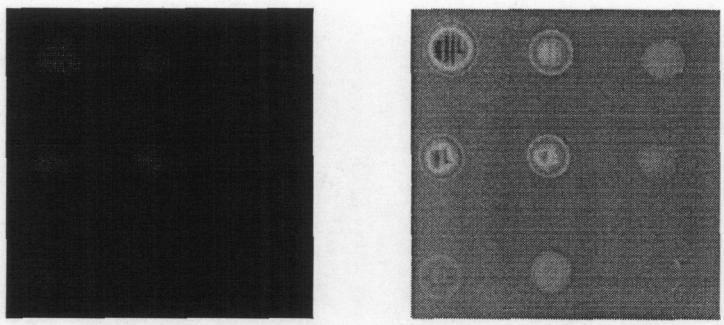

Figure 2.5: Droplet Fluorescence. Left: Actual fluorescence spectrum from the BSA in each of the droplet from Figure 2.4. Right: A color enhanced view of the droplets depicting the actual fluorescence intensity [1].

Figure 2.5 above is a view of the fluorescence intensity from each of the droplets. Digital enhancing the fluorescence map, as is done on the right of the figure, very clearly shows the variation among the droplets due to their volume of BSA. Knowing the amount of BSA injected into each droplet and the intensity of the fluorescence from each, the fluorescence versus concentration plot in figure 2.6 was produced. From this plot a relation can be derived to perform the reverse experiment in which the protein concentration is the unknown. This is one possible detection method to be employed in the PFP device.

circuitry would be benign. Based on previous experience with the material, Poly (dimethylsiloxane), or PDMS, was deemed the best-suited material for this application.

3.1 General Design

MD Anderson's experimental setup for evaluating the dielectrophoresis effect on droplets was the origin of many design considerations. This setup used drawn glass micropipettes to inject droplets onto microscale electrodes patterned on a glass substrate by LLNL. The micropipettes were attached to micrometers to allow for precise control of their position with respect to the electrodes. (Figure 3.2)

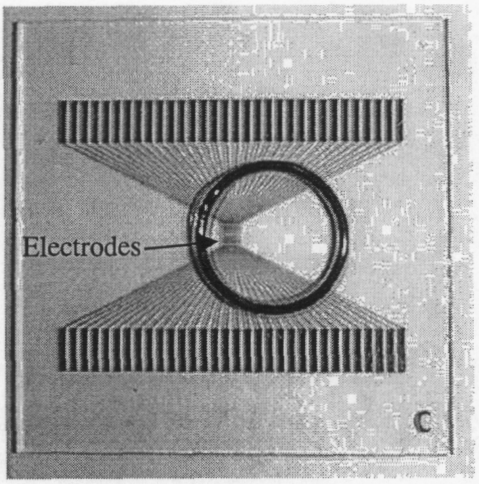

Figure 3.1: Electrodes surrounded by bromododecane dam. Bromododecane is the medium used to contain the droplets during manipulation.

A small rubber o-ring was glued to the glass substrate to surround the electrodes as shown in Figure 3.1. The o-ring served to contain the bromododecane in which the droplets would be manipulated. The bromododecane medium was necessary because it allowed the droplets to be polarized and therefore susceptible to the DEP forces from the electrodes. Since water is immiscible in bromododecane, the droplets were suspended in

the fluid above the electrodes. Thin leads were patterned from the electrodes to larger scale contact pads. These pads were interfaced with conductive Zebra connectors (Fujipoly America, Carteret, NJ) and connected by a ribbon cable to a PC board on which the glass substrate was fixed. Figure 3.2 shows this setup with the external electronics connected to the PC board.

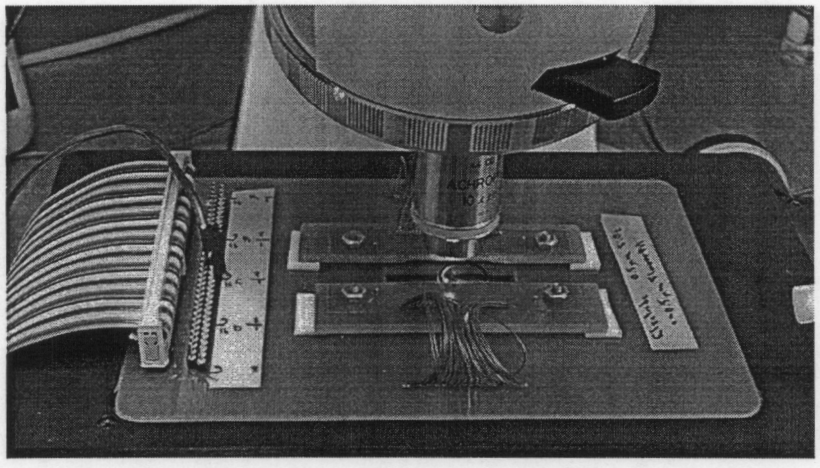

Figure 3.2: Experimental setup including connection to external electronics.

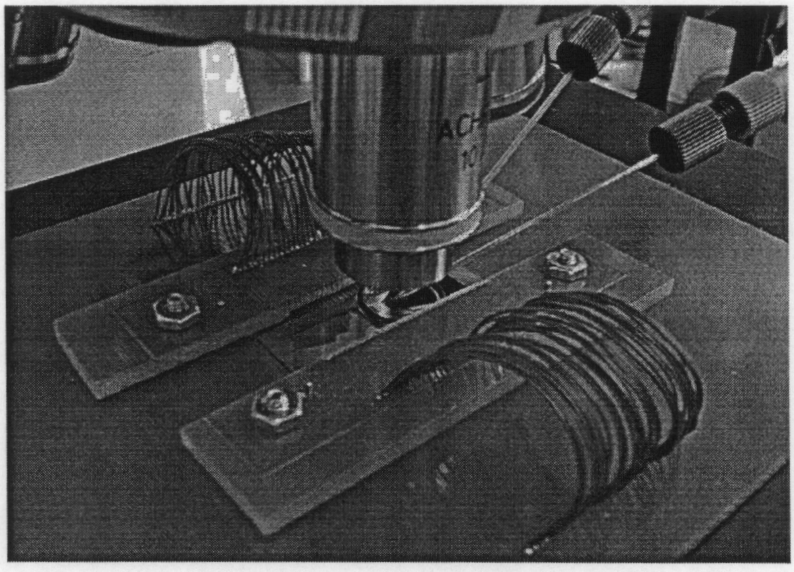

Figure 3.3: Experimental setup with micropipettes positioned over electrodes.

The first generation microfabricated device was employed primarily to evaluate fabrication techniques and for proof-of-principle regarding the microfluidic injection system. The design integrated the droplet injectors and electrodes from the original test apparatus. Aspects such as the size and spacing of the contact pads were maintained in order to use the same Zebra connectors for linking to the external electronics. The major design changes involved the fabrication of a microfluidic system directly onto the substrate containing the electrodes and the use of a package to facilitate the external electrical and fluidic connections.

Figure 3.4 is a model of the first generation design, including the PFP device, circuit board, and package. The device's microfluidic system consisted of an inlet port, storage chamber, injection channels, and the PFP chamber containing the electrodes. The magnification in Figure 3.4 shows the location of the injection channels with respect to the array of electrodes.

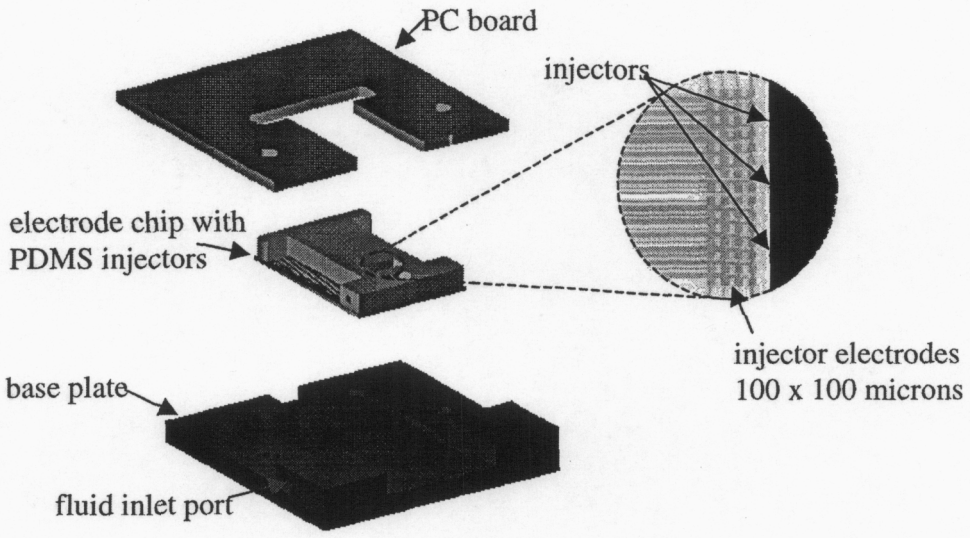

Figure 3.4: Exploded model of the first generation device, package, and pc board.

The PC board shown in Figure 3.5 was designed to have convenient test points connected via traces to contact pads aligned with the Zebra connectors on the PFP device. These test points were included to provide better access for controlling the electrodes during experimentation.

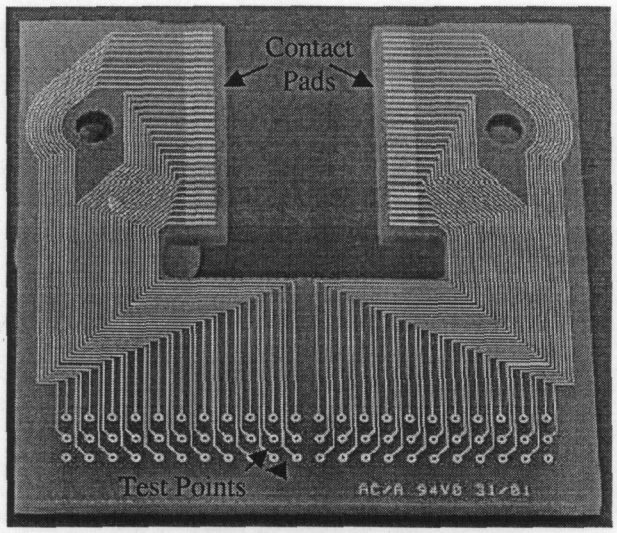

Figure 3.5: PC Board used between the PFP device and control electronics.

A simple package was developed with a baseplate to hold the device. The device and Zebra connectors were sandwiched between the PC board and base plate to provide adequate downward pressure on the PC board for maximum electrical contact. The base plate also included a threaded port for installing an Upchurch connector to facilitate fluid connections to the device.

3.2 Design Experimentation

The specific design of features such as electrode dimensions, passivation layer thicknesses, and the size of the injection orifice into the PFP chamber were determined by experimentation and/or modeling. MD Anderson conducted experiments with sample

substrates from LLNL and Coventor Inc. developed models to simulate the effect of the features in question. This preliminary work was done in order to reduce the number of iterations necessary in fabricating these critical elements.

3.2.1 Electrodes Design

In order to optimize electrode performance when manipulating droplets, it was necessary to determine an appropriate geometry to generate the largest DEP force while minimizing the voltage needed. Lower voltages not only reduced the power required for the device, but it expanded the options for the integrated circuit structure. The electrode geometry was selected based on experimental and theoretical results. Experimentation consisted of three electrode geometries patterned at similar size scales. These shapes included stars, crosses, and squares. From qualitative analysis of droplet movement seen through a microscope, the square electrodes appeared to be the best.

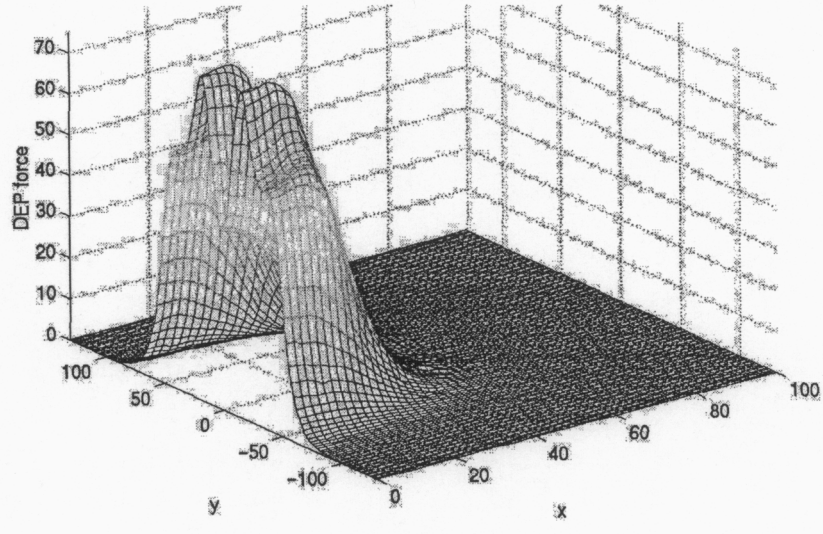

Figure 3.6: Model of the DEP forces from a single square electrode [7].

This qualitative analysis was supported by Coventor's model of the DEP force distribution on a 30 μm square electrode, shown graphically in Figure 3.6. Because the force emerges from the edges of the electrode, it was apparent that a square was better suited than a star or cross due to the larger side length and proximity of the edge forces between adjacent electrodes. When moving droplets along the array, it is beneficial to have four edges that can exhibit high DEP forces in order to attract the droplet to the next electrode in the desired direction.

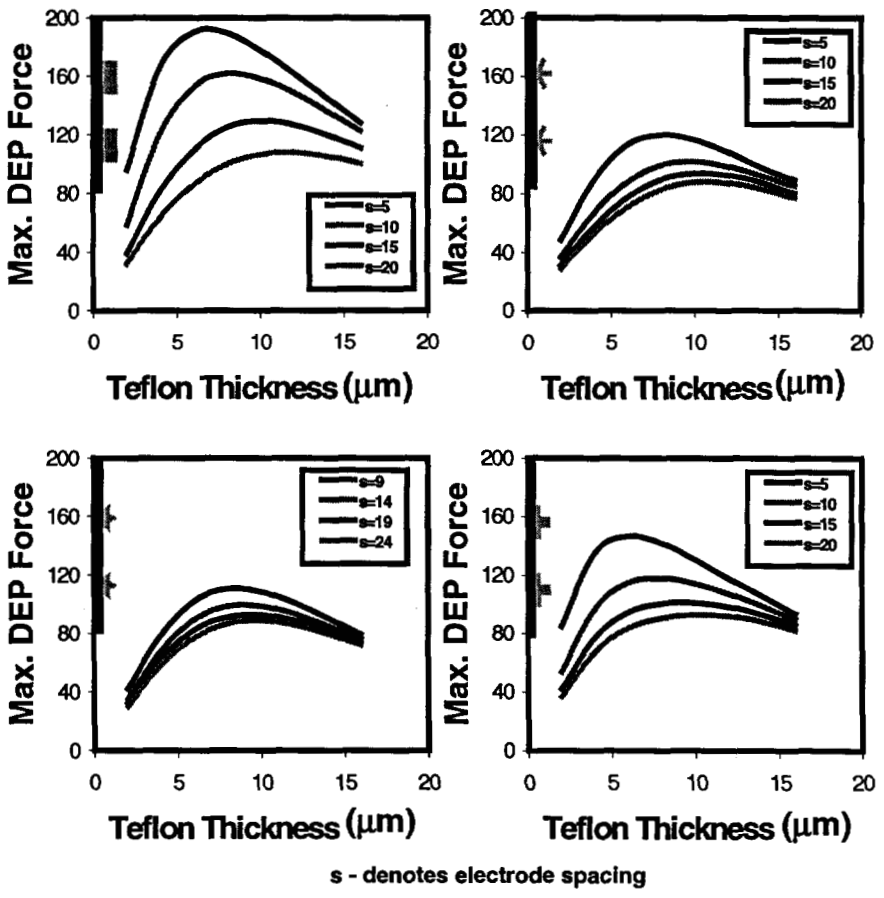

Figure 3.7: Results from experiments to determine the optimal electrode shape and Teflon passivation layer thickness. The electrode shape for each plot is denoted on the y-axis by a representative cross-section. Each curve corresponds to a different spacing between adjacent electrodes [7].

Coventor produced models of various electrode geometries and passivation thicknesses to estimate the achievable DEP forces. This data, shown in Figure 3.7, also shows that the square geometry (noted along the y-axis) elicits the highest DEP force through a Teflon passivation layer. Similar results would be expected for other passivation materials as the force curve would exhibit the same characteristics with an altered magnitude.

3.2.2 Passivation Layer

Once the electrode geometry was established, the passivation layer separating the electrodes and the droplets was examined. This layer provides a gap between the droplets and the electrodes to create a capacitance. It was therefore necessary for this material field from the electrode to affect the droplet without allowing direct contact of the droplets to the metal. If a droplet were to simultaneously come in direct contact with two electrodes it would short the drive electronics. These device specifications required examination of material properties such as dielectric constant, breakdown voltage, adhesion, and film uniformity when fabricated. The thickness of the layer was also an important design consideration. Referring to Figure 3.7 above, important aspects of the Teflon thickness can be deduced. For example, the DEP force decreases monotonically with the separation distance and peaks for a thickness between 4 and 10 μm. It is important to pinpoint the distance at which the force peaks because the voltage necessary to drive an electrode can be reduced for thinner layers.

MD Anderson performed a qualitative analysis of the passivation characteristics of PECVD SiO2, parylene, and diamond-like carbon. The results from their analysis are in Table 3.1. Based on this data, they determined that silicon dioxide with a thin layer of

parylene was the most favorable passivation layer due to its hydrophobic surface and ability to withstand voltages in the anticipated operating range.

Surface Coating	Qualitative Results
830 nm PECVD SiO_2	held off 120 V
300 nm SiO_2 with 1 um parylene	parylene provides a nice hydrophobic surface
1 um parylene	withstood sufficient voltage and is currently the coating of choice
laser ablated diamond-like carbon, different thicknesses	DLC is slightly conductive and shorts electrodes

Table 3.1: Results of experimentation with SiO_2, parylene, and diamond-like carbon to be used as passivation layers

Diamond-like carbon was not feasible because it was found to be slightly conductive, allowing droplets to short adjacent electrodes. Although hydrophilic, silicon dioxide did hold off the high voltages and was selected for the first generation design. This selection decision incorporated the fact that SiO_2 is commonly used as a final insulation layer in microelectronics fabrication and would therefore correlate well to an integrated device design.

3.2.3 Droplet Holdoff Pressure

Jon Schwartz of MD Anderson did testing to determine the pressure at which droplets would spontaneously eject from their micropipettes [8]. This information was important for the injector design because it provided input as to the appropriate injector orifice diameter as well as an operating range for the pressure in the device. Figure 3.8 from MD Anderson depicts a hypothetical pressure drop in a pipette at different stages during the droplet injection process.

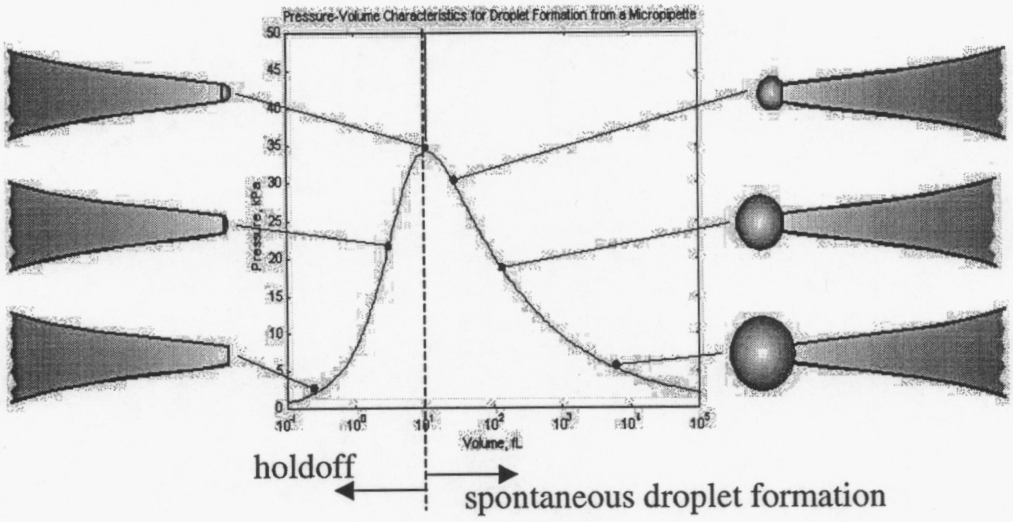

Figure 3.8: Droplet pressure with a changing radius due to increased volume. The peak pressure occurs when the droplet is hemispherical, after which formation is spontaneous [8].

Equation (1) describes the pressure needed to inject a droplet from the micropipette, where γ is surface energy based on the fluid and the medium into which it is injected, and r is the radius of the droplet as it grows.

$$\Delta P = \frac{2\gamma}{r} \tag{1}$$

The volume of the droplet is dependent on the radius and size of the droplet relative to the orifice size. These variables are depicted in Figure 3.9 and their contribution to the volume is shown in Equation (2).

$$Volume = \pi a^2 (r - \tfrac{1}{3} a) \tag{2}$$

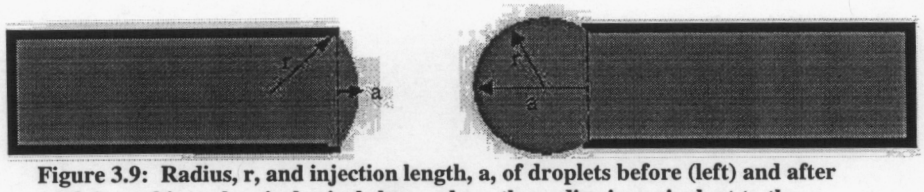

Figure 3.9: Radius, r, and injection length, a, of droplets before (left) and after (right) reaching a hemispherical shape where the radius is equivalent to the injection length.

Because the surface energy is constant, only the radius of the droplet determines ejection pressure. Initially the radius of the droplet is infinite, and therefore there is no pressure needed to maintain the droplet at this geometry. As the droplet grows to a hemisphere, the radius gradually decreases and the pressure needed to maintain the droplet at that radius increases. Once the droplet is hemispherical, a maximum amount of pressure is necessary to hold the droplet at that radius, corresponding to half the micropipette diameter. If any pressure is added to the droplet, spontaneous growth will occur as the radius increases and the pressure required decreases. The droplet will release from the micropipette in order to minimize its energy in a spherical shape. The maximum, or holdoff, pressure needed to eject droplets could be determined by measuring the pressure at which droplets were released from a micropipette.

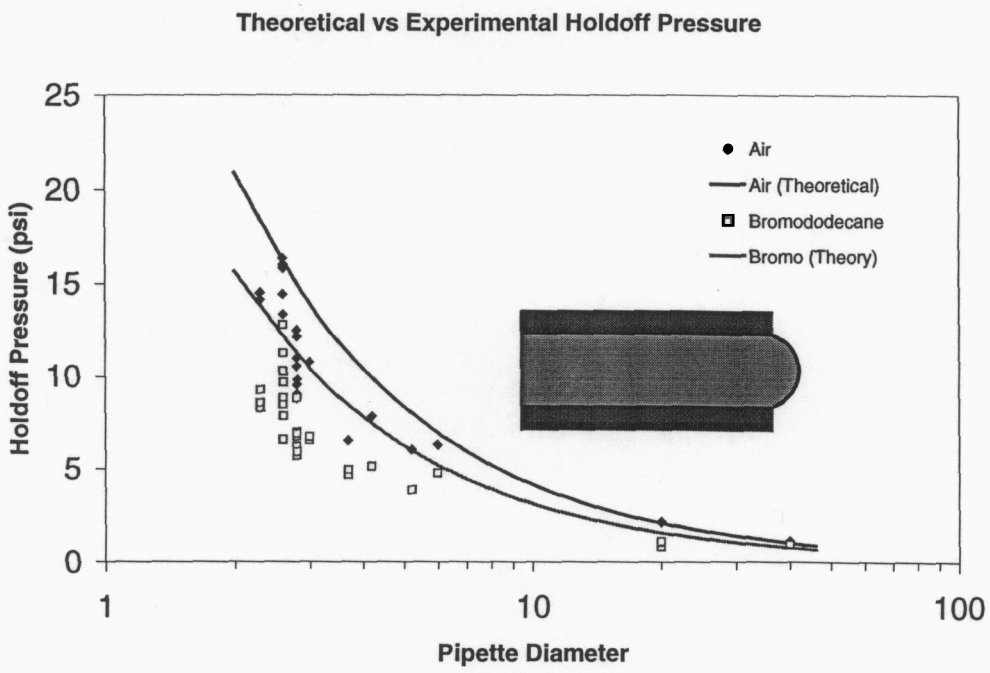

Figure 3.10: Hold pressure for various micropipette diameters, based on the inner diameter [8].

The design of the orifice for the injectors was determined from experiments done by MD Anderson using several different pipette diameters. This experiment determined the holdoff pressure for different pipette diameters, therefore providing additional information as to the appropriate orifice size. The surface energy of the fluid in air and bromododecane could also be extracted from a curve fit of this data. Figure 3.10 shows a plot of this data based on the inside diameter of each pipette tested. A shift was apparent between the experimental data and theoretical data with established values for surface energies. To eliminate this disparity, the data was recalculated using the outer diameters as depicted in Figure 3.11. Using this outer diameter provided a much more accurate fit between the theoretical and experimental values.

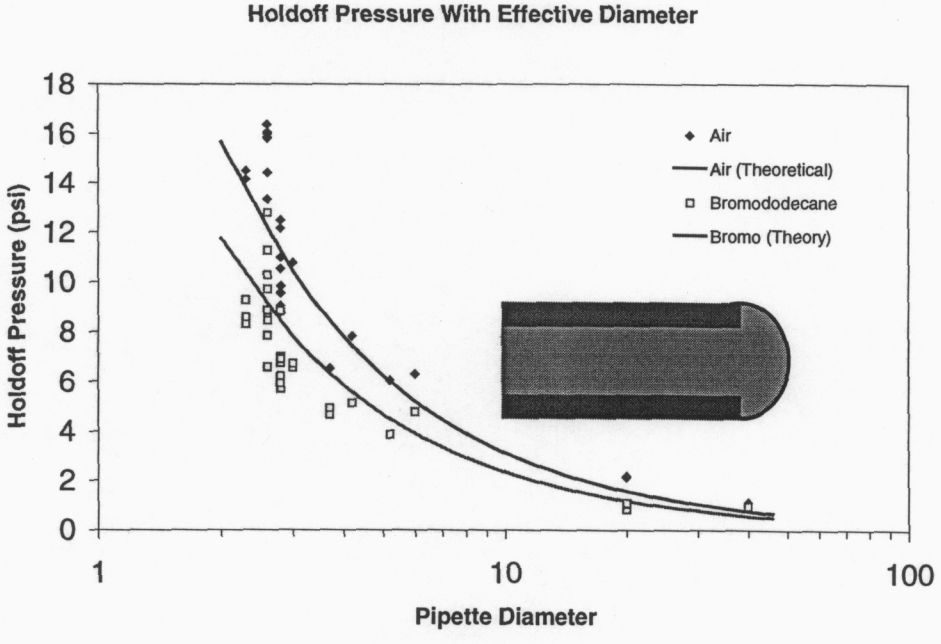

Figure 3.11: Hold pressure for various micropipette diameters, based on the outer diameter.

The droplet shift to the outer diameter was a potential hindrance in designing the PFP device if droplets expanded in a similar manner from injector orifice. Unlike a

micropipette with a tip inner and outer diameter, the injector in the PFP device was designed to be a hold emerging from a planar surface. The concern was that droplets might become extremely large as they expanded upon this planar surface until they reached an edge. After qualitative analysis of droplets from injectors, it was determined that the inner diameter of the injectors would in fact determine the radius of the droplets and therefore drive the pressure dependence.

4 First Generation Fabrication

Combining the information collected from MD Anderson's experimentation and Coventor's modeling with LLNL's fabrication experience, the design for the first generation PFP device was finalized. It was then necessary to focus on the fabrication materials and processes that would be used. The novel modifications made to established process techniques required multiple stages of trial-and-error before ascertaining the most appropriate technique. Although these iterations were time intensive in the first generation, they led to a robust design and process flow for subsequent generations. The original process flow for the first generation device, complete with detailed process parameters, is located in Appendix A, and the general process is described below.

4.1 Substrate

The substrate chosen for fabrication was Borofloat® glass, a borosilicate glass commonly used in microfluidic applications due to its chemical, electrical, and optical properties. According to the manufacturer (Schott Corporation: Yonkers, NY), exposure of Borofloat® glass to water and acids results in small amounts of monovalent ions leaching out of the glass. This leaching creates a thin non-porous silica coating on the surface of the glass making the surface nearly impermeable during future fluid exposure. Borofloat® glass is also a suitable insulator for avoiding electrical shorting of patterned surface electrodes due to low alkali (Sodium and Potassium) content [9]. The optical

transparency of glass was advantageous for the first two generations of devices because it allowed for inspection of all parts of the system with a standard microscope.

The substrate was cleaned in a piranha (1:1 H_2SO_4/H_20) solution to remove all impurities from the surface and to initialize the formation of the non-porous silica coating. Dehydration at 120 °C ensured uniform surface coating during proceeding photolithography steps.

4.2 Electrodes

An electrode array was patterned on the surface of the glass substrate in order to perform dielectrophoresis for droplet movement. Each electrode required a connection to an individual contact pad near the edge of the device for testing purposes. As seen in the expansion of Figure 4.1 below, an array containing four rows of fifteen electrodes was designed with 100 μm square electrodes spaced 100 μm apart. These dimensions were chosen based on testing performed by MD Anderson using similar arrays to determine optimal size, shape, and spacing of electrodes.

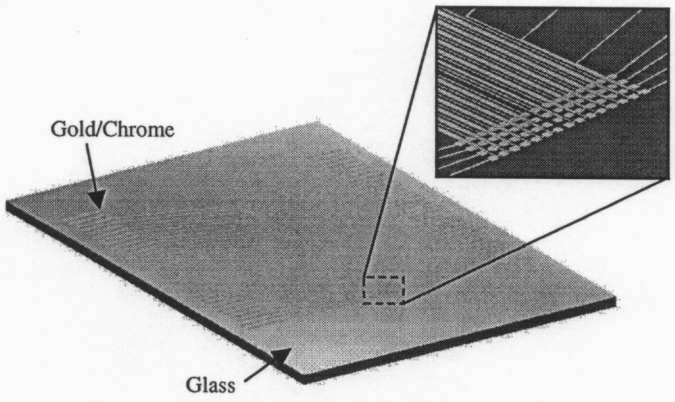

Figure 4.1: Gold electrodes patterned onto glass substrate.

The thin leads connecting the electrodes to the pads were designed to be approximately 10 μm wide, sized much smaller than the electrodes to avoid interference with the DEP forces. Due to the spacing of the electrode array, up to four traces were designed to run in parallel between two electrodes. If these traces were too large and a voltage was simultaneously applied to each of their respective electrodes the traces would mimic an electrode and disrupt control of the DEP forces.

The electrodes were patterned onto the glass substrate using the "liftoff" process. In this process, photoresist was lithographically patterned on the surface using a glass photomask. The photoresist was then soaked in chlorobenzene to create the edge profile depicted in Figure 4.2. A 200 Å adhesion layer of Chromium and a thin 2000 Å layer of Gold were evaporated over the patterned photoresist, adhering to the glass surface in the clear regions. Removal of the resist and the unnecessary metals in an acetone bath revealed the desired pattern. This process has been fine-tuned to create precise features as small as 2 μm and is therefore well suited for this application. The electrodes were fabricated in a class 100 clean room and special care was taken to avoid any inadvertent contamination during processing as even a microscopic impurity between the glass and metal could create a gap in the thin 10 μm leads, eliminating electrical contact to an electrode.

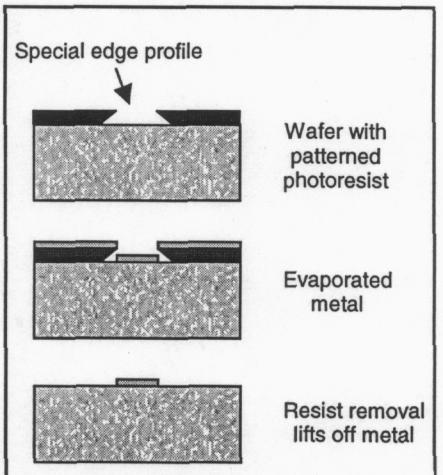

Figure 4.2: Lift-off Process

4.3 Passivation Layer

A passivation layer was required on the patterned electrodes to avoid shorting of the electrical circuits when contacted by ionized droplets and while maintaining the maximum DEP force achievable on the droplets. Several passivation materials were tested to determine the optimal dielectric properties; however fabrication of the first generation preceded these tests. In the first generation, silicon dioxide was used based on its known properties and common use as an insulator in semiconductor manufacturing. The use of SiO_2 also seemed appropriate as it mimicked the final microelectronic layer expected in the ultimate device design and can be deposited at relatively low temperatures. This makes it compatible with the processes

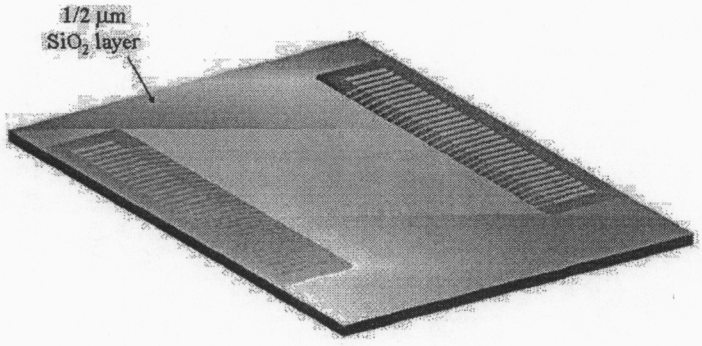

Figure 4.3: Patterned SiO2 layer over the electrodes and traces.

A thin 500 nm layer of oxide was grown on the glass substrate using plasma-enhanced chemical vapor deposition (PECVD). In order to make sufficient electrical contact with the test pads, the oxide was removed in this region. This was done by patterning a protective layer of photoresist, then etching the oxide in a plasma of 80% CF_4 and 20% O_2. The electrodes were tested manually to ensure that the oxide had been sufficiently removed.

4.4 Injection Channels

The fluid system for the first generation device included microchannel injectors connecting an externally loaded storage chamber with the PFP chamber where dielectrophoresis was performed. The small diameter of these microchannels aids in creating droplets when fluid is forced through the system in pressure flow. Based on MD Anderson's experimentation with droplet formation from micropipettes, the dimensions of the channel orifice were chosen as a 2, 5, and 10μm square as well as the rectangular combinations of these sizes. This range was chosen to provide an indication of the correlation between ejection pressures for a square or rectangular orifice versus similar collected data for a circular orifice in a micropipette. This square geometry was settled on through extensive modeling by Coventor on the orifice effect on final droplet geometry. They found that rectangular orifice produced droplets that were comparable to a circular orifice whose diameter matched the smaller side length of the rectangle. Similarly, a square orifice was found to eject droplets with dimensions matching those of a droplet from a circular diameter equal to the square side length.

The other important decision was to allow the substrate to act as the bottom wall of the channel, the simplest solution in terms of fabrication. Discussions on this topic surmised that contact with the substrate would not adversely affect the droplets as they emerged from the channels as long as the bottom surface was hydrophobic. The length dimension was chosen based on the amount of surface area around the fill chamber necessary for bonding a cover layer and ignored fluid effects. The full dimensions of each channel injectors were therefore 2, 5, and 10μm square by 5mm long between the two chambers. Not only were the channel dimensions critical, as they would be used to

establish the optimal dimensions for future generations, but the alignment of the channels with regard to the electrodes was critical as well. Two axes of alignment were requested by MD Anderson to facilitate their DEP testing. The first was the alignment of the injector orifice with respect to D_1 in Figure 4.4, representing the distance between the injector and the beginning of the electrode array.

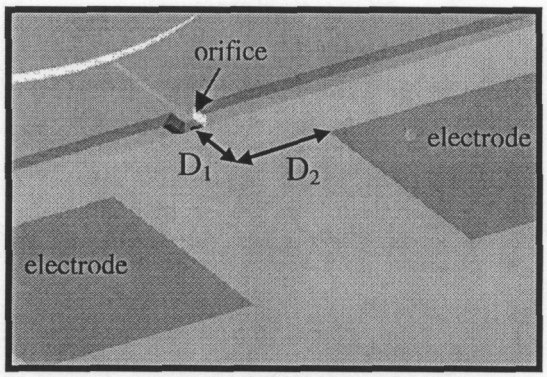

Figure 4.4: Electrode alignment with respect to the injector orifice.

This distance was requested to be 50, 100, and 200 μm in separate devices to determine the effect of DEP on a droplet at the orifice. The second alignment was with respect to D_2. MD Anderson requested two variations: one with the center of an electrode aligned with the orifice, and the second with the electrode gap aligned with the orifice as shown in the figure. These two alignments were intended to provide data on the most favorable position for receiving an injected droplet and the effect of orifice alignment on the DEP forces.

4.4.1 Etching methods

To achieve alignment between PDMS and metal features to within a tolerance of ± 5 μm, the strategy was to pattern the injectors in a method similar to other surface

micromachining techniques. This first called for the channel patterns, three 5 μm wide by 5 mm long lines for example in Figure 4.5, to be patterned on the substrate using a photoresist approximately 5 μm thick. These lines were placed on the surface within ± 5 μm of their desired location using alignment features on the substrate to align the subsequent photomask.

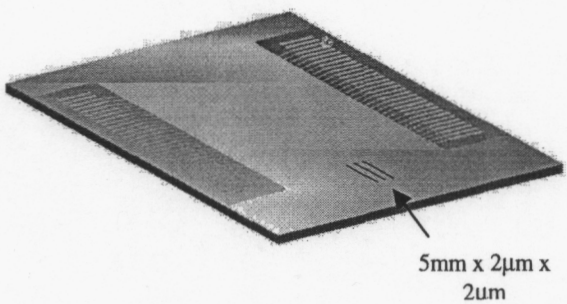

Figure 4.5: Photoresist lines patterned on the SiO_2 to be used for molding injectors.

PDMS polymer was spun onto the substrate, at a thickness calculated from the related spin speed. This 20-30 μm thick polymer covered the entire substrate, including the three photoresist lines, as shown in Figure 4.6A.

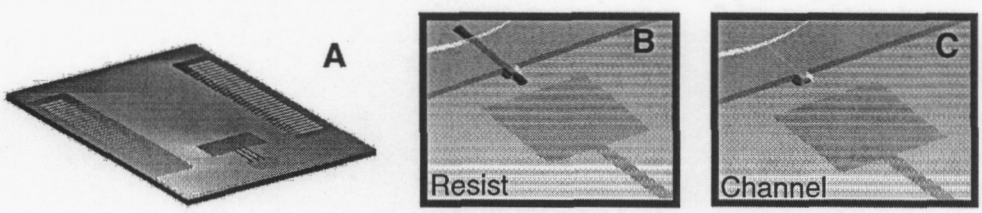

Figure 4.6: Model of the method for producing the desired channels in PDMS. A: Patterned PDMS covering the photoresist lines. B: Close-up view of the resist beneath the PDMS. C: Channel formed after removal of photoresist line.

After curing of the polymer, a standard AZ® photoresist was patterned on the surface to provide a masking layer during etching. This etching step was intended to pattern the

initial opening for the PFP and storage chambers, and remove material from the test pad areas. Once these regions were removed, creating the pattern seen in Figure 4.6B, the photoresist could be removed from the substrate creating a channel in the polymer as in Figure 4.6C.

The polymer was etched in a reactive ion etcher with plasma composed of 80% CF_4 and 20% O_2. Due to the slow etch rate of the polymer, approximately .5 μm/min, the masking layer of photoresist was not robust enough to withstand the long etch times necessary to reached the desired depth.

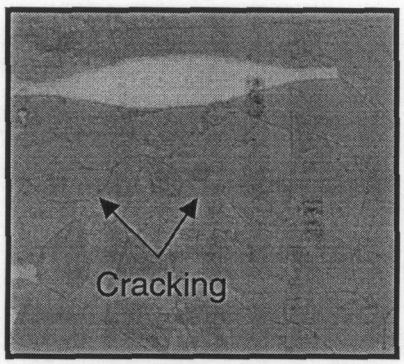

Figure 4.7: Cracking in the photoresist layer patterned onto a thin layer of PMDS.

It initially was believed that the plasma etch was causing the photoresist cracking seen in Figure 4.7 above; however, it was ascertained through experimentation that the hard bake required during photolithography was actually the cause. The presumption was that the chemical content of the PDMS was reacting with the photoresist as both layers out-gassed during the 120 °C hardbake. This step could not be eliminated because it was required in order to have the photoresist withstand the plasma etch. The inferred solution was therefore a more robust photoresist that could withstand the harsh etch conditions and did not require a hard bake. This led to a thick laminated photoresist that could be pressed onto the polymer film. Once applied to the surface, the resist was patterned using

standard photolithography methods to create a masking layer for the features. Although the resist was much thicker and therefore more resilient to the plasma etch, delamination of the resist coupled with consistent contamination of the plasma system during the polymer etch, led to abandonment of this approach.

4.4.2 SU-8 techniques

To eliminate the patterning problems encountered with using a PDMS film to form the injector channels, a new material was evaluated as a substitute. The properties of SU-8 (Microchem Corp: Newton, MA) epoxy based photoresist allow it to be patterned at high aspect ratios, with feature thicknesses much greater than their width or length. The processing required is similar to photolithography with standard photoresists, although different chemicals are used and a post exposure bake is necessary. As was done within the PDMS process, three 5 μm x 5 μm x 5mm lines were patterned on the glass substrate with AZ® photoresist. SU-8 was then spun over the entire substrate to a desired thickness. The SU-8 was successfully patterned to create the open regions over the electrodes, contact pads, and storage chamber base. The underlying photoresist forming the channels was then removed in an acetone bath. Inspection of the channel regions confirmed that the photoresist had been entirely removed leaving well-formed channels.

With this achievement, the molded PDMS forming the bulk of the fluid chambers was to be bonded onto the SU-8 layer. PDMS would not bond to SU-8, however, without a thin titanium adhesion layer between the materials. This requirement proved to be yet another impediment because the titanium would have to be patterned on the SU-8

surface. A liftoff process similar to that used for patterning the DEP electrodes was employed for patterning the titanium into the areas to be bonded and to mask other from the titanium. When attempting to remove the photoresist and unwanted metal, acetone was ineffective at removing titanium from the substrate surface in some regions. One affected region was the PFP chamber containing the metal electrodes. Residual titanium in this area was a potential means for shorting the electrical connections in the system. This method was consequently deserted.

4.4.3 Spin patterning methods

As an alternative to etching and using other materials, an intriguing polymer patterning technique developed by Duffy et al. [10] and diagramed in Figure 4.8, was experimented with.

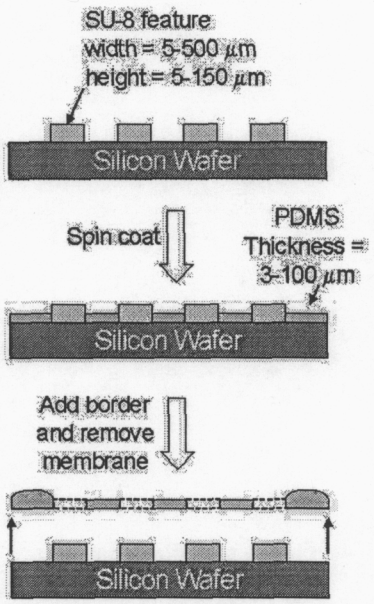

Figure 4.8: Diagram of PDMS patterning process as described by Duffy et al. [10]

The group used SU-8 photoresist to create 50 μm tall posts with 50 μm diameters on a silicon substrate. They then spun on a layer of PDMS with a thickness below the height of the posts. A PDMS ring was poured around the edge of the wafer to allow for removal of the membrane without damage. The PDMS was then cured and the membrane was removed from the silicon substrate. This membrane was implemented as a reusable "dry liftoff" mask for patterning metals on various substrates. The flexibility and tackiness of the polymer material allows for reversible adherence to substrate surfaces, providing a seal with the substrate sufficient for patterning metals. The results from their experiments showed precisely pattern columns with 50 μm diameters in a PDMS film. These images spawned interest in the applicability of this approach to the PFP device because it was a potential means for patterning a PDMS film without etching.

This approach was not directly applicable to the PFP device, but a variation of the process was promising. Instead of using permanent posts and removing the PMDS film, it was necessary to remove the photoresist features from the substrate leaving a patterned PDMS film. Alignment would be nearly impossible if the film was lifted from the molding substrate, and then bonded to the PFP substrate but would be very precise if the photoresist could be removed instead. The other major difference was the scale at which the PDMS parts needed to be patterned. The published experiments had been done with features only as large as 150 μm tall with a 500 μm diameter whereas the main area of the PFP device would be on the order of square millimeters.

Several experiments were performed to test the viability of these process variations. Since the straight walled mold features obtainable with SU-8 resists would provide the best feature geometry, an experiment was done to see if this material could be

removed from a substrate after it was patterned. Films of SU-8 from 20 μm to 250 μm thick were patterned on separate glass substrates in an inverse design of the desired PDMS area. These films were then left in an acetone bath over a fifteen-minute period. Films less than 50 μm curled up, softened, and released from the surface while thicker films tended to curl at the edges, but maintain most adhesion area with the substrate. This data limited the potential height of the PDMS film because it could only be spun on at fraction of the thickness of the SU-8 for the patterning process to work.

PDMS was then spun onto a substrate with a mold formed by 50 μm thick patterned SU-8. The PDMS thickness was pre-determined by spin-rate analysis shown in Appendix C. Although thickness variations were made in this experiment they were irrelevant because the SU-8 processing sufficiently contaminated the substrate surface and prevented adhesion of the PDMS membranes. All membrane thicknesses lifted off the substrate when placed in the acetone bath.

To alleviate this contamination problem, an enhanced polymer photoresist, photo-patternable up to 75 μm was investigated. Clariant's AZ PLP-100 was patterned on the surface using a method similar to that explained for other polymer resists used in the processing. The resist was patterned to create a reverse image of the desired polymer areas on the substrate. These features were approximately 50-60 μm thick to allow for relatively thick polymer layers. PDMS was spun onto the surface as explained above, then cured and qualitatively analyzed for adherence to the substrate

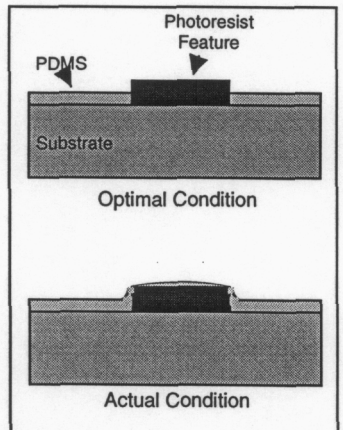

Figure 4.9: Residual PDMS over photoresist patterned features

in clear areas. While the PDMS did adhere well to the substrate, it did leave a thin membrane over the photoresist features as sketched in Figure 4.9. When the photoresist was removed with acetone, these 1-2 μm polymer films created jagged edges at the intersection of the photoresist and the clear regions as they ripped during their release. The rough edges were not acceptable for this device, because of alignment issues and anticipated chaotic interactions of the fluid with the edges without a precisely patterned film. This process was therefore abandoned for this project due to feasibility issues.

4.4.4 Molding methods

During the initial design phase of this project, the feasibility of using a PDMS molding method similar to the soft lithography method had been discussed. In this process, the channel design would be patterned out of photoresist, molded into PDMS, and bonded to the glass substrate containing the electrodes. Due to alignment issues however, it was decided that this approach was less favorable than patterning the PDMS directly on the substrate. After experimenting with two separate patterning methods as was described above, the molding approach was revisited.

The large fluidic components of the device, including the fluid storage chamber and PFP chamber, were already intended to be molded using acrylic molds. (This process is explained in length in the following section.) The photoresist lines that form the injector microchannels were therefore patterned directly onto the bottom section of the mold between the storage and PFP chambers as seen in Figure 4.10. This was accomplished by first exposing the bottom acrylic plate to an oxygen plasma to allow the photoresist to wet the surface when spun on. The three photoresist lines were then patterned on the

acrylic surface. Due to a lack of any alignment feature in this process, the photoresist lines were imprecisely positioned.

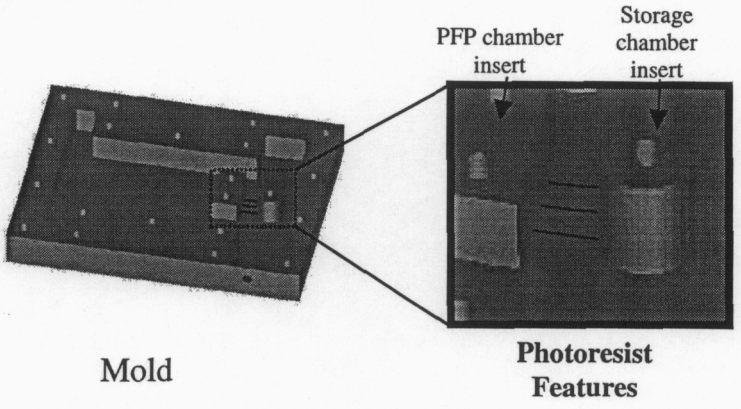

Figure 4.10: Mold with photoresist lines patterned between the storage chamber and PFP chamber inserts.

The mold was then assembled, filled with the polymer precursor, and baked to cure the PDMS. Upon removal from the mold, the region of the polymer having been in contact with the photoresist was rinsed with acetone and isopropyl alcohol to remove any residual resist that could cause blocking in the channels. The PDMS block was then roughly aligned to the electrodes on the glass substrate and bonded. A small glass square was also bonded over the storage chamber to seal it.

A filter was placed inline with a water filled syringe to test the flow through the channels without introducing any potentially disrupting particles. The devices tested all failed due to pressure leakage before they exhibited any droplet ejection. This failure occurred at the interface between the PDMS and the glass cover over the storage chamber due to a lack of adequate surface area for adhesion. These high pressures were caused by clogging in the extremely long, narrow channel that had been designed for the device.

The channels were even narrower than their designed 5 by 5μm cross-section due to the inability to pattern high aspect ratios with standard polymer photoresist.

Both problems were addressed by once again utilizing the epoxy based SU-8 photoresist. The SU-8 resist could not be patterned directly onto the acrylic mold, so a 3-inch round wafer was employed instead. This wafer would contain the photoresist injector lines, and would replace the acrylic as the bottom layer of the mold. The photoresist lines were patterned onto the surface at a 5 μm thickness. These lines did not adhere well to the glass though due to their extremely small surface in contact with the substrate. Data from the manufacturer revealed that typical surface treatments used to promote photoresist adhesion only aggravated the problem.

Because the high pressures had also been a problem with the small cross-sections, it was determined that using larger channels (20 by 20 μm) could eliminate both the adhesion and pressure problems. These larger channels would be suitable substitutes for this generation because they would answer the question of whether this design would yield droplets. These larger 20 μm cross-section lines were therefore patterned on a 3-inch round glass wafer as described above. The resist lines remained adhered to the surface throughout the processing. The glass wafer clipped to the rest of the acrylic mold and roughly aligned so that the photoresist lines were between the storage and PFP chambers. The polymer was injected into the mold and cured. This molded block was approximately aligned to the electrodes on the glass substrate and bonded. The approach proved successful for creating devices from which valuable information could be extracted for designing the second-generation devices.

4.5 Device Scale Molding

Fabrication of the large polymer features of the device, shown bonded to a glass substrate in Figure 4.11, was done using an acrylic mold.

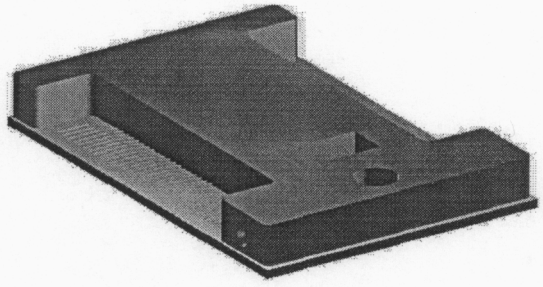

Figure 4.11: Bulk fluidic features molded in PDMS using and acrylic mold

The acrylic material was specially chosen because it did not interact with the PDMS material to be molded. Due to water absorption and chemical composition, many acrylics will contaminate the polymer and inhibit curing, but the acrylic material used in this application did not exhibit these detrimental characteristics. Molds were fabricated in an automated circuit board milling machine to ensure accurate dimensions of the features. The acrylic mold consisted of three layers, as shown in Figure 4.12, and joined together by screws into the tapped center layer.

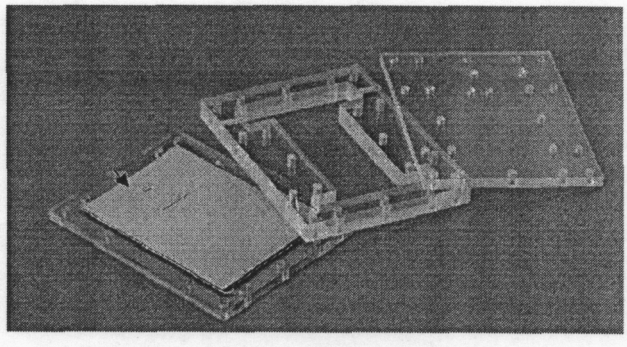

Figure 4.12: Example of an acrylic mold used for casting the bulk PMDS parts.

The bottom and top layer were nearly identical, and contained the through holes for attaching the two acrylic inserts. These inserts were used to mold the cylindrical storage chamber as well as the rectangular PFP chamber. The inserts (Figure 4.13) were ¼ inch thick, identical to the center acrylic layer, with a diameter of 5 mm for the cylinder and approximately a 5mm by 10 mm face on the rectangle.

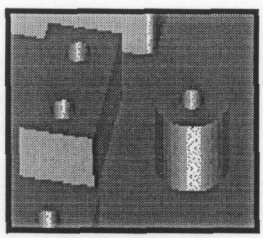

Figure 4.13: Mold inserts for patterning the PFP and storage chambers.

A fluidic channel for loading the sample fluid was created using hollow metal pins with Teflon tubing running through them to the center of the cylindrical insert. This created a molded pathway between the external fluid port on the package and the storage chamber molded by the cylindrical insert.

The pre-polymer mixture was thoroughly mixed and degassed, then injected into the assembled mold through a small hole in the top acrylic layer. The injection was done at a relatively slow rate to avoid creating permanent bubbles in the polymer. Once injected, the mold was placed in an oven at 60 °C for one hour to cure the polymer. Once cured, the PDMS was removed from the mold, with caution taken to avoid contaminating the surface to be in contact with the glass substrate with the patterned electrode.

Attaching of the PDMS took advantage of the covalent bond achievable between PDMS and glass. The bonding surfaces were rinsed in ethanol to ensure the removal of all contaminates, and then placed in an oxygen plasma to activate the surface molecules [3]. Using a delayed bonding strategy, the parts were then completely immersed in

methanol for five minutes [11]. The parts were removed and placed in conformal contact, using a microscope to aid in the rough alignment of the molded features to the electrodes on the substrate. Evaporation of the methanol was achieved by placing the glass directly onto a hotplate, and a permanent bond between the two materials was achieved. Using this approach, a well-aligned set of PDMS features with respect to the surface electrodes is not possible because the PDMS required hand alignment to the glass substrate. By modifying this process to include alignment features on the bonding surfaces, the technique was vastly improved for the second generation device.

4.6 Chamber Capping

Sealing the storage chamber is necessary to build a large enough pressure to form droplets from the injectors and to force these droplets beyond the geometrical threshold at which they release spontaneously. This seal was made using a simple glass rectangle of the appropriate dimensions to cover the storage chamber. Similar to the previous bonding processes, the glass and PDMS surface were rinsed with ethanol to remove all contaminants and placed in an oxygen plasma for one minute. The glass was then pressed into position to form the irreversible bond over the chamber.

5 First Generation Results

After a great deal of modifications to the process flow during fabrication of the first generation devices, a viable approach was finally implemented to produce working devices. First generation devices were sent to MD Anderson for experimental feedback in designing the next generation. Other devices were analyzed by LLNL to determine necessary design changes to improve fabrication as well as device function. An example of a completed device is shown below in Figure 5.1.

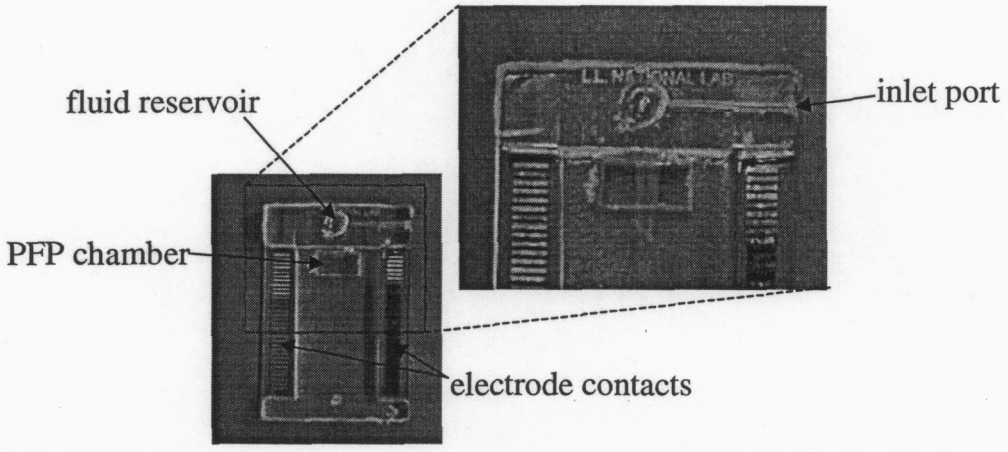

Figure 5.1: Example of a completed first generation device.

Using the information from MD Anderson's testing and the knowledge of problems encountered during fabrication at LLNL, proposed changes were discussed between the collaborators. These problems ranged from breaks in the electrode traces to a method for accurately aligning the microfluidic features to the electronics. For each problem, an appropriate solution or an experiment necessary to obtain a solution was constructed. These problems are discussed in the following sections. Modifications were integrated into the design and process flow for the second-generation device.

5.1 Breaks in Electrode Traces

Because the first and second-generation devices were to be hybridized with the electronics placed off-chip, a means of transmitting signals to the electrodes was necessary. Contact to the chip was made to large gold pads along the edge of the device using Zebra connectors in contact with a powered PC board. From each of these pads a 10 μm wide line was patterned to intersect an individual electrode. (Figure 5.2) Due to the placement of the electrodes and the pads, many of the 10 μm wide lines were as long as two centimeters as they ran along the device. Despite precautions taken during the photolithography steps used to create these traces, their dimensions made them very susceptible to gaps caused by particles or other contaminants. Any gap along a trace would break the electrical circuit rendering the attached electrode inoperable.

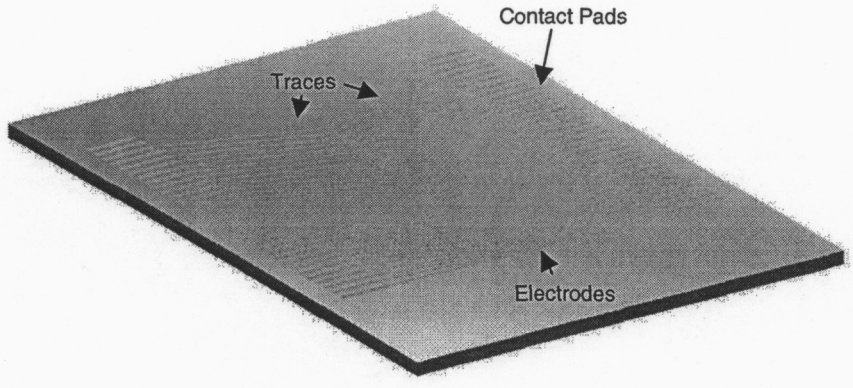

Figure 5.2: Model of the patterned metal electrodes, contact pads, and traces.

During fabrication of the first generation devices, each device was inspected under a microscope following the photolithography step to confirm that no particles were evident along the trace paths. This only ensured that contamination during photolithography

would not be an issue, but did not account for the likelihood of contaminants during deposition of the metals.

5.2 Droplet Formation Pressures

The final first generation devices ejected droplets into the PFP chamber with an externally applied pressure of less than 1 psi, a range that would require very sensitive pressure control. This low injection pressure was the result of using larger channels, 20 by 20 μm cross section, to eliminate adhesion problems of the storage chamber cap under high pressures. The original design of 4400 μm long channels with a 5 by 5 μm cross-section required pressures greater than 30 psi, far beyond the adhesion strength of the bond between the PDMS and the glass over the storage chamber. At pressures this high, leaks developed from the storage chamber reducing the holdoff pressure well below 5 psi. The high aspect ratio of the channels was also a concern due to the increased tendency to clog. It was necessary to design injectors for the second generation devices that would eliminate clogging while maintaining pressures in the desired operating range.

5.3 Optical Distortion During Experimentation

The array of 100-micron electrodes was placed near the edge of the PFP chamber in order to locate the electrodes in close proximity to the droplet injectors. This required that the 5.7 mm thick PFP chamber be filled with the suspending fluid (bromododecane) and sealed with a cover slip in order to view the electrodes. With the well only partially filled, and without a cover slip, the suspending fluid formed a meniscus at the wall of the

well, grossly distorting the microscope image of the electrodes. Because the oily suspending fluid is slightly dispersive, a 5.7 mm deep pool of bromododecane tended to blur the image of the electrodes, and presumably, the image of any droplets sitting on the electrodes. This slight distortion was acceptable to test the first generation injectors but required a more convenient solution for the next devices.

5.4 Injector Fabrication

After extensive iterations involving the fabrication of the droplet injectors, it was decided that the method of molding the injectors was most promising. This method used SU-8 patterned injectors on a 3 inch round glass wafer. This wafer replaced the original acrylic as the bottom layer of the mold. The glass wafer clipped to the rest of the acrylic mold and roughly aligned with it so that the photoresist lines were between the storage and PFP chambers. This rough alignment was not acceptable for the second generation devices, which required the injector to electrode alignment to be within ±5 μm. The method of clipping the glass wafer was also very crude and demanded a more repeatable and robust approach.

5.5 Fluid Reservoir Evacuation

During testing of the devices it was discovered that a means was needed for evacuating air from the fluid reservoir in which the solution was stored. With only an inlet port leading to the storage chamber, air became trapped in the reservoir forming

bubbles in the fluid. Because these bubbles could disrupt the flow through the injection channels a design alteration was needed in order to make this evacuation much simpler.

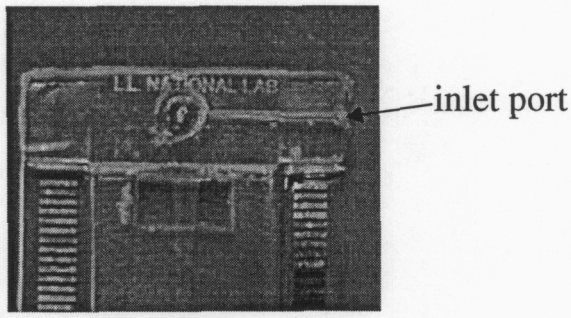

Figure 5.3: Fluid port used to fill and evacuate fluid storage chamber.

5.6 Microfluidics to Electrode Alignment

MD Anderson's design requirements specified two variations of the lateral electrode alignment with respect to the injector. The first was to have the gap between two electrodes centered on the injector, and the second had a single electrode centered on the injector. These variations were to be used in determining the appropriate alignment for pulling droplets with DEP forces from the injectors' openings. They also wanted to have various distances between the injector and the first row of electrodes to experiment with the amount of DEP force that would be needed to eject a droplet. Neither of these alignments could be accomplished with the rough alignment procedure used in the first generation. Placement of the PDMS containing the injector channels was done by hand with the aid of a microscope, but this resulted in approximate alignments off by up to 500 μm in either direction. While this was sufficient alignment for the first generation in which the critical function was pressure driven droplet ejection, modification was necessary to obtain precise alignments for the second generation.

5.7 Surface Coating

The silicon dioxide passivation layer between the droplets in solution and the surface electrodes prevented shorting of adjacent electrodes by mutual droplets. The coating did however produce the undesired effect of a hydrophilic surface in the PFP chamber. Droplets injected onto the surface could not be controlled by DEP forces because they tended to wet the chamber surface instead of maintaining their spherical shape. A thin film of hydrophobic fluoropel was used to coat the injection channels and PFP chamber surface in order to run experiments. This coating was effective for extracting data during brief trials, but subsequent experiments required a new coating to recreate the hydrophobic effects.

5.8 Storage Chamber Capping

The glass section bonded over the fluid storage chamber allowed for the pressure buildup needed to force a droplet out of the injector. Due however to the small amount of bonding surface area, the glass could not withstand high pressures. Once the seal between he glass and PDMS had been broken, even small pressures were not achievable due to fluid leakage.

The lack of compliance in the glass meant that if too much pressure were applied, droplets would be injected until the pressure decreased below the hold-off threshold. This was a major problem because the pressure of the system needed to be maintained within a pre-determined range during operation. This problem was studied using modeling and experimentation while designing the second-generation device.

6 Second Generation Design

The second-generation device was a hybrid design with the microfluidic system patterned onto a substrate containing electrodes controlled by separate integrated circuits. The design of the device, as well as the process flow for fabrication, was based on the data obtained during fabrication and testing of the first generation.

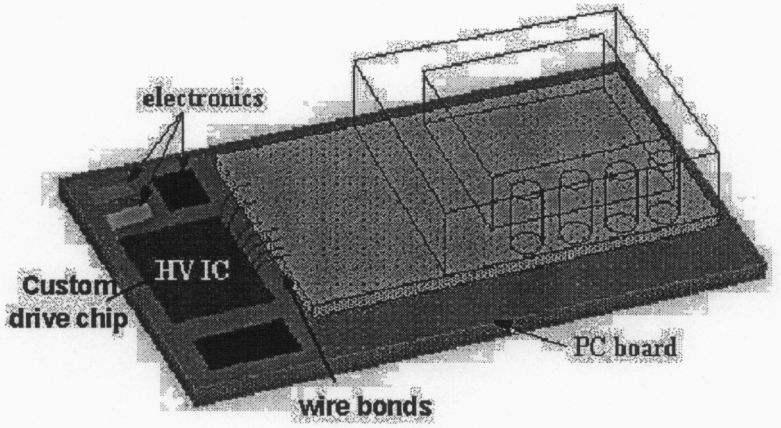

Figure 6.1: Anticipated design of a hybrid second-generation device with the high voltage integrated circuits and microfluidics patterned on separate substrates.

Similar to the first generation, many of these modifications required experimentation and modeling to determine the optimal design choice. Design and testing of the second-generation integrated circuits was maintained separately from the microfluidics with the intention of combining the components in a means similar to Figure 6.1.

6.1 Package

While many changes were made to the second generation device, only one change was made to the package and associated parts. The polymer-based microfluidics were

once again bonded onto a glass substrate containing the electrodes. The electronics were connected using the Zebra connectors between the chip and the PC board. The package from the first generation was reused to minimize changes necessary in the test setup. The only change made to the package was a rectangular hole milled out of the bottom to provide viewing of the droplets on the electrodes. This eliminated the distortion problems caused by viewing the droplets through the large volume of slightly dispersive bromododecane.

6.2 Qualitative Design Changes

Several design changes were instituted based directly on the results from the first generation and without any need for extensive modeling or experimentation. These modifications were a result of testing performed by MD Anderson on the first generation devices as well as specific concerns that arose during fabrication of the original device. Several changes were made to the electrode and trace patterns as well as the passivation layer and mediatory fluidics.

6.2.1 Electrode Traces

The fragility of the long 10 μm traces connecting the electrodes to contact pads on the edge of the chip was a major concern from the first design. There was potential for one of these trace paths to be interrupted by a contaminating particle during fabrication. No charge and therefore no DEP force would be available to the electrode. While this was not an issue for the integrated device in which the electrodes would be powered from

integrated circuits directly below, the problem could potentially inhibit the test of the second-generation device.

The new design employed two modifications in an attempt to decrease the likelihood of particles fully disrupting the conducting traces. First, the length of all the traces was decreased. Instead of running the traces along the center axis for long distances, the shortest path from an electrode to contact pad was used. Special care was taken during the design to ensure that adequate distance was maintained between adjacent traces as they angled away from the densely populated region near the electrodes. The resulting pattern is shown below (Figure 6.2) in comparison to the first generation.

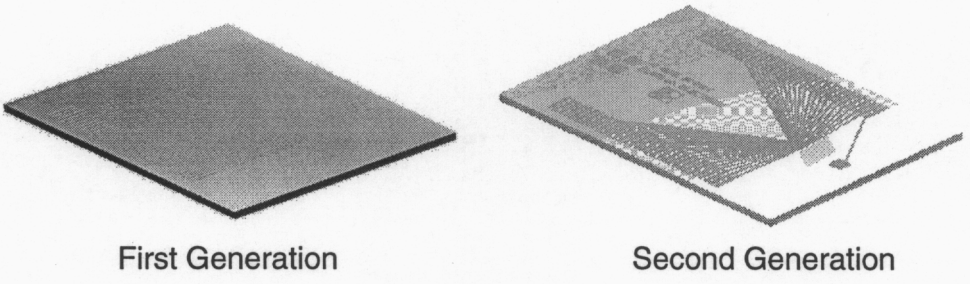

Figure 6.2: Comparison of first and second-generation electrodes designs.

The second modification made to the traces was to taper them from 10 μm near the electrodes to 500 μm at the intersection with the contact pad. Increasing the width of the traces on the substrate greatly reduced the probability of a particle completely disrupting the conduction path.

6.2.2 Ground Electrode

Another change made to the electrode pattern was the addition of a 3mm by 3mm square electrode beneath the fluid storage chamber. This distinct electrode is apparent in

the electrode model for the second generation shown in Figure 6.2 above. This electrode was used to ground the test solution before injecting it into the PFP chamber for manipulation. Grounding the solution ensured that droplets injected into the PFP chamber initially had no net charge. A conducting trace connected the electrode to a contact pad from the original array used in the first generation. This eliminated any need for modification to the packaging and external electronics.

6.2.3 Outlet Port

It was necessary to include a means of purging air from the reservoir during filling for the second generation device. The simple solution to this problem was to incorporate an outlet port from the storage chamber to a connection with the external package. This port was designed as a mirror image of the inlet port and was to be fabricated using identical means.

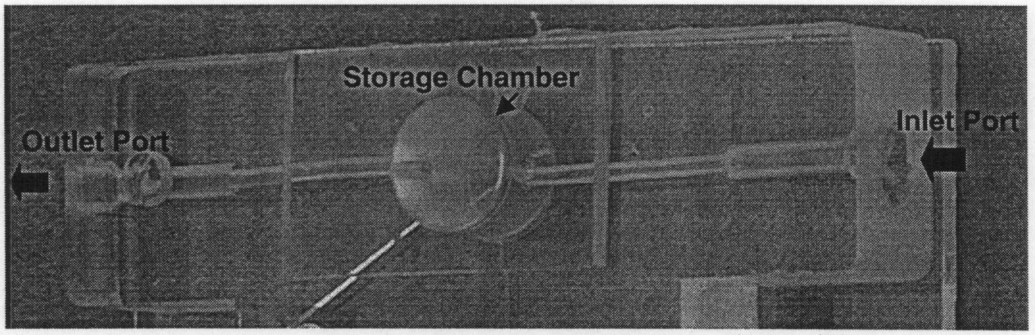

Figure 6.3: Inlet and outlet ports allowing for filling and evacuation of fluid storage chamber

6.2.4 Surface Coating

The silicon dioxide surface coating used as a passivation layer over the DEP electrodes disrupted formation of droplets in the PFP chamber and created an undesired

flow profile in the injector channels due to its hydrophilic nature. The droplets injected onto the silicon dioxide surface tended to wet the surface instead of holding their spherical shape. This surface wetting also affected flow through the injector channels. Both the observed and the desired flow profiles are shown in Figure 6.4. The three PDMS walls surrounding each flow channel were hydrophobic, having a contact angle greater than 90 degrees. The silicon dioxide layer, forming the bottom wall of the channel, was hydrophilic and would therefore tend to pull the fluid through while the other three walls were impeding flow.

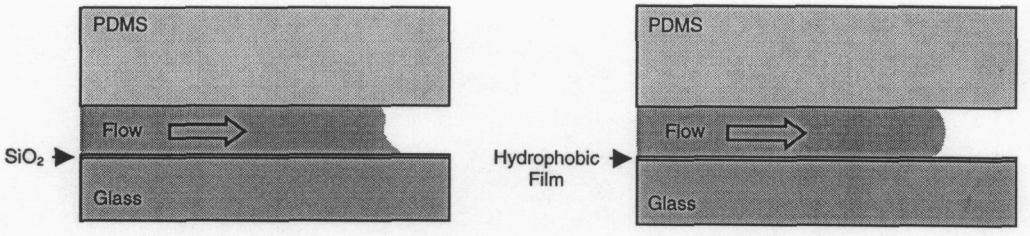

Figure 6.4: Estimated flow profiles through the injection channel. Left: Flow profile with a hydrophilic SiO_2 passivation layer. Right: Flow profile with a hydrophobic passivation layer.

This produced an irregular flow profile that hindered the formation of droplets, as they tended to wick onto the electrode surface. The desired flow profile, shown on the right in Figure 6.4, has four hydrophobic walls and results in droplets that will maintain their spherical shape once entering into the PFP chamber. This flow problem necessitated a change in the material used, specifically one that could provide the favorable passivation properties of silicon dioxide, but with a hydrophobic surface.

While several hydrophobic passivation layers were feasible, it was desirable to have all four walls with nearly exact hydrophobic qualities. Parylene, a conformal polymer that can be vapor-deposited onto the walls of the injection channel, was selected.

This provided a uniform contact angle along all four of the channel walls as well as a hydrophobic surface in the PFP chamber.

6.3 Experimentation and Modeling Design Changes

Based on the feedback from the first generation device, modeling was needed to determine the effects of suggested design changes to the microfluidic features of the device. The models and crucial parameters were verified with experimentation and through references to previous research. Using these tools, the design for the microchannel injectors and the pressure storage system were analyzed and improved.

6.3.1 Injector Channels

In an attempt to reduce the overall fluidic system pressure during filling and injection, the contributing phenomena were modeled to pinpoint potential dimensional or material changes that could be made. The large pressure necessary to produce droplets from the injectors was the result of blockages in the channel as well as viscous and surface energy effects along the channel walls during filling. A model of each of these effects was produced for the straight channel and compared to a proposed in-plane taper design. Although it would produce lower pressure, a three-dimensional taper was not possible due to the planar limitations of the microfabrication methods. A comparison of the two designs is shown Figure 6.5 below.

The tapered section was designed to intersect with a short region of straight channel near the injection orifice. As in the original design, the final width was the same

as the height of the channel, creating a square orifice. In the models, widths of the straight and tapered regions were variable, as well as their lengths. This allowed for comparison of the effects of several different taper designs.

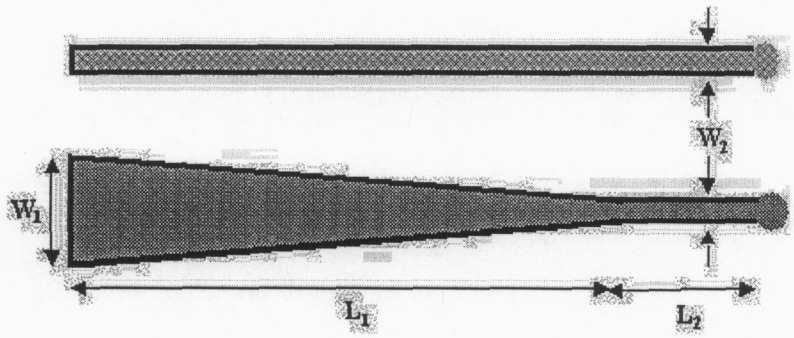

Figure 6.5: Straight and tapered channel profiles. The straight profile was utilized in the first generation. The tapered design was instituted for the second generation to decrease fill pressures and avoid clogging issues.

6.3.1.1 Viscous Pressure

The first model created was of the viscous effects along the walls while filling the channels. Equation (1) was used to describe the pressure drop, P_v, along the channel due to the viscous effects.

$$P_v = f\frac{L}{D_h}\frac{\rho\bar{V}^2}{2} \tag{1}$$

The pressure drop is dependent on the density of the fluid, ρ, and a dimensional quantity, L/D_h, relating the length of the channel to the hydraulic diameter. Hydraulic diameter is calculated based on the cross sectional area, A_c, and the wetted perimeter, P_w, of the channel.

$$D_h = \frac{4A_c}{P_w} \tag{2}$$

The tapered region in the new design had a decreasing hydraulic diameter as the channel width decreased. The average velocity, $\overline{V}$, was estimated using reasonable values of fill velocities in the range of 100 μm/s to 1 mm/s and affected not only the pressure drop, but the friction factor, f, as well. The friction factor is dependent on whether the flow present in the channel is laminar or turbulent. The Reynolds number is used to determine the type of flow in the channel, and can be calculated using Equation (3).

$$\mathrm{Re} = \frac{\rho V D_h}{\mu} \tag{3}$$

The variables are the same as used in the pressure drop equation above, with the addition of a dynamic viscosity variable, μ. If the Reynolds number is less than a value of 2300, then laminar flow can be expected in the pipe. As is the case with most microfluidic systems, the Reynolds numbers for these channels were typically between 1 to 5 and therefore laminar. The laminar flows have a friction factor dependent solely on the value of the Reynolds number, as opposed to turbulent flows whose friction factor is related to the wall roughness. Equation (4) describes this dependence on the Reynolds number.

$$f = \frac{64}{\mathrm{Re}} \tag{4}$$

Using this data, the viscous pressure drop was modeled as the fluid filled the channel. Comparisons were made of the results from various taper and straight lengths as well as different taper widths. Figure 6.6 shows a plot for one 5 mm long channels both with a constant height of 2 μm, and with final widths of 2 μm as well. The tapered region had an initial width of 100 μm and decreased linearly along the 4 mm taper length to the final 2 μm width. The velocity used in this simulation was 1 mm/s, a reasonable flow compared to anticipated values for the actual device. This speed was used to

determine a worse case scenario for viscous pressures in the system. The effect of the taper on the viscous pressure drop was dramatic. Pressures above 1-2 psi have a significant impact on the microfluidic system due to the amount of pressure needed to release a droplet (explained in detail in section 6.3.1.3).

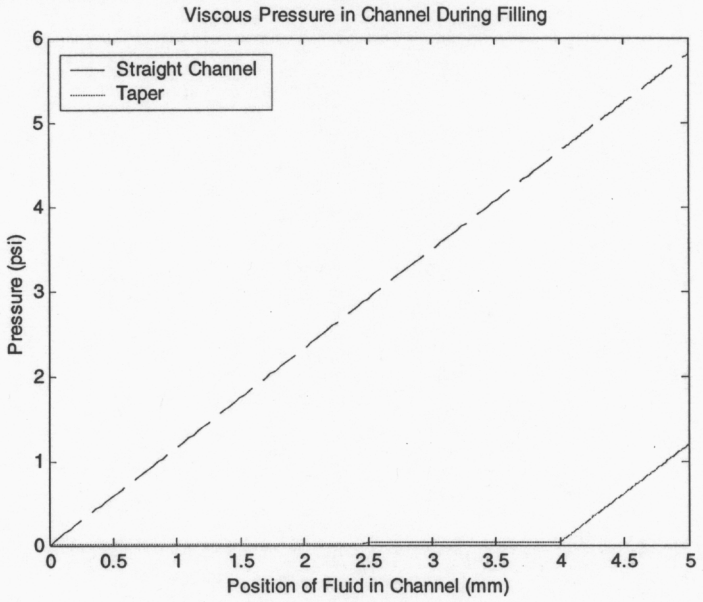

Figure 6.6: Viscous pressure in a straight and tapered channel of equal length.

As seen in Figure 6.6, the viscous pressure created along the 5mm long, 2 μm square channel was in the 6 psi range. The goal of the design was to reduce the viscous pressure below 1psi, which was effectively done using the 100 μm to 2 μm taper for the simulation. This final pressure drop could be further reduced in the simulation by shortening the length of the straight region near the injector orifice.

6.3.1.2 Wetting Pressure

The second pressure considered for the model was the wetting pressure from capillary forces developed during filling of the channel. This pressure is due to the

interaction of the fluid's surface energy as well as the hydrophobic or hydrophilic nature of the channel walls. This pressure drop is described by Equation (5),

$$P_w = \frac{2\gamma}{r}\cos\theta \tag{5}$$

where γ is the surface energy of the fluid relative to the medium in which it is contacting, r is the radius of the channel, taken to be half the hydraulic diameter in this case, and θ is the contact angle of the fluid when touching the channel wall. The surface energy values were taken from the experiments performed by MD Anderson and are described in Section 3.2.3. The calculated surface energy values of water in air and bromododecane were .075 N/m and .084 N/m respectively. Using values from literature, a contact angle of 110 degrees for water on PDMS [12] and 87 degrees for water on parylene [13] were used in the simulation.

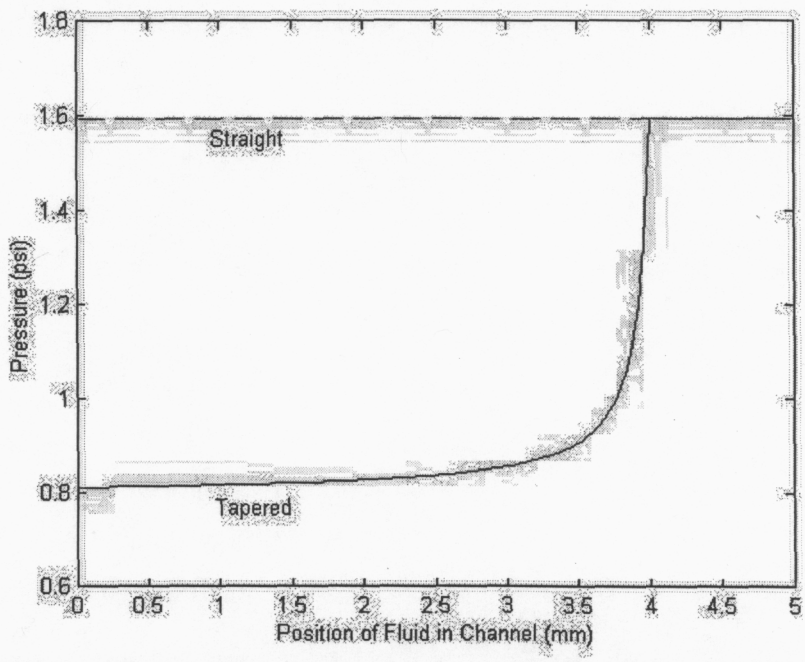

Figure 6.7: Wetting pressure in straight and tapered PDMS channels of equal length.

An assessment of the wetting pressure model revealed the effects of a tapered region followed by a straight region. The inverse dependence on the hydraulic radius of the channel means that as the tapered width decreased, the pressure increased. In non-tapered channel sections, the wetting pressure is a constant. The implication of this relationship is that the taper has no effect on the wetting pressure near the injector orifice. Instead, the use of a small straight section prior to the orifice creates a final wetting pressure equal to that of a non-tapered channel.

This wetting pressure data was combined with the viscous pressure data to model the overall pressure while filling the channel, as shown in Figure 6.8.

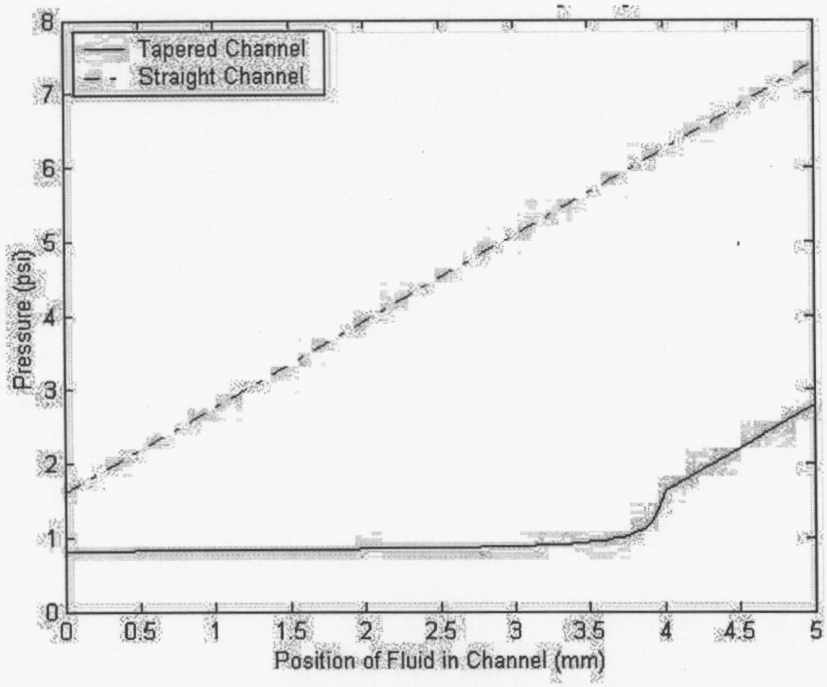

Figure 6.8: Total fill pressures for straight and tapered channels.

The pressure to fill the channel could not be reduced to a trivial value due to the wetting pressure at the end of the channel, but the taper did provide a dramatic change in the overall fill pressure. The 4 mm long 100 μm to 2 μm taper followed by a 1 mm long

straight section had an overall pressure drop in the channel of less than 3 psi. This value was much less than the approximate 7.5 psi necessary for the non-tapered 5 mm long and 2μm wide channel. This reduction put the pressure well below the droplet ejection peak pressure, as described in section 6.3.1.3, achieving the desired goal from altering the channel design.

6.3.1.3 Droplet Growth

A large pressure was needed in order to eject a droplet into the bromododecane medium occupying the PFP chamber. The origin of this large pressure depends on surface energy considerations. The equation for the ejection pressure was simply,

$$P_e = \frac{2\gamma}{r} \tag{6}$$

where γ was once again the surface energy of the fluid relative to its surrounding medium, and r is the radius of a droplet as it emerges from the injector.

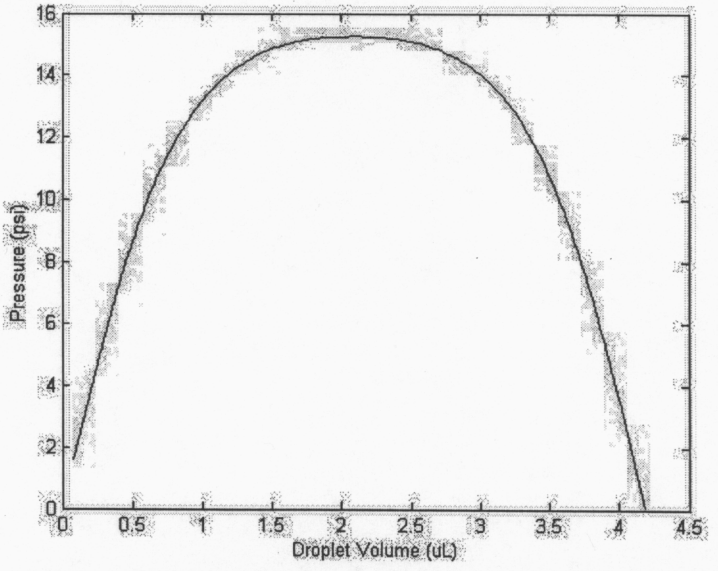

Figure 6.9: Droplet ejection pressure for a 2 μm injection orifice.

Using a 2 μm orifice diameter and a surface energy of .072 N/m for ejection of a water droplet into air, the plot in Figure 6.9 was created for pressure during droplet growth. This ejection pressure had no dependence on whether the channel was tapered or straight, only on the final orifice diameter. The orifice diameter corresponds to the minimum radius of a droplet, at which the pressure is maximized. The pressure needed to eject a droplet was much higher than the pressures developed during filling of the channel. Although this high pressure was assumed to be much less significant during design of the first generation it was an important feature to prevent the ejection of residual droplets due to pressures from filling the channel. As discussed in section 3.2.3, once the maximum pressure was reached, corresponding to a hemispherical droplet, a spherical droplet would spontaneously grow. This observation was used in the analysis of a fluid capacitor for maintaining pressure in the system.

6.3.2 Fluid "Capacitor"

The pressure data pertaining to droplet growth showed that individual droplets could be injected into the PFP chamber by increasing the pressure to just beyond a peek value for the orifice diameter. If the system pressure was maintained above this peek, many droplets would be injected onto the surface or a large droplet would grow until the pressure would drop below a threshold value. MD Anderson developed the solution to this control problem of using DEP forces to provide the necessary energy to promote spontaneous droplet formation. Application of this force effectively bypassed the peek pressure to produce spontaneous droplet growth. This effect is portrayed in Figure 6.10,

with the droplet exceeding the hemispherical threshold without an additional drive pressure.

The next step was to establish the minimum drive pressure needed to support the DEP effect and the maximum drive pressure at which the droplets were hemispherical. These values provided a range between which the microfluidic system was to be operated. The driving pressure for the injection system was applied at the storage chamber which lost volume when after each droplet injection. It was necessary to maintain the drive pressure within a specific range despite these volume changes.

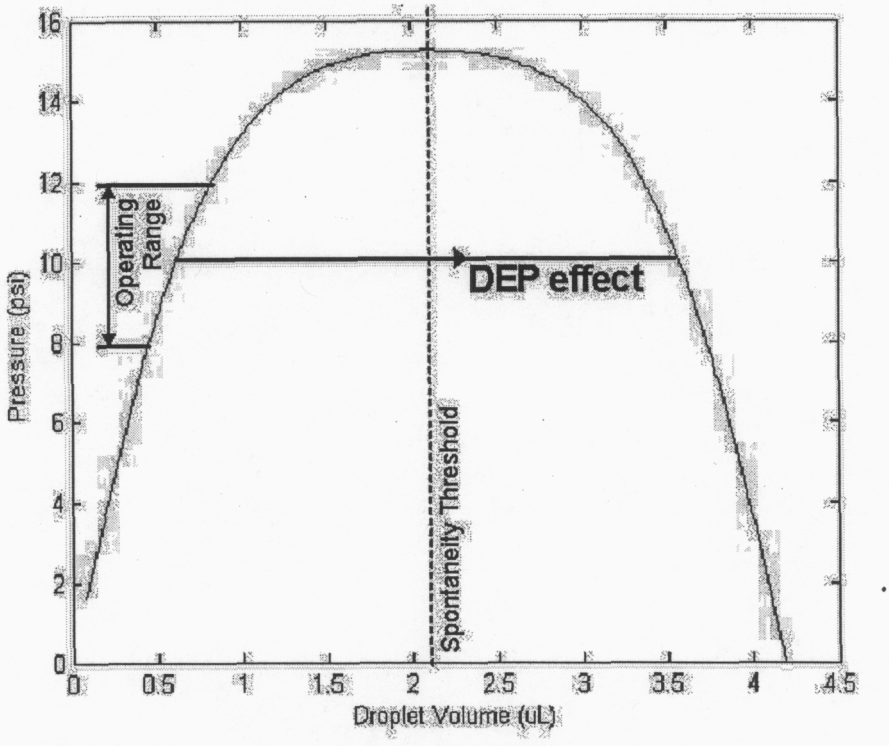

Figure 6.10: DEP effect on droplet formation. This chart also includes a hypothetical operational range for the system pressure and the spontaneity threshold past which droplets surface tension forms spherical droplets.

To maintain a relatively constant pressure despite volume losses, a flexible membrane similar to Figure 6.11, was designed to cover the storage chamber. This membrane was

to be patterned from PDMS to a thickness determined via simulation. This membrane was a replacement for the stiff glass piece previously used to seal the fluid storage chamber.

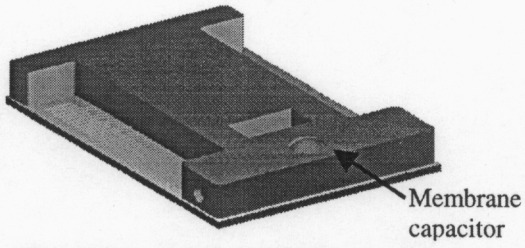

Figure 6.11: Model of the design for a flexible membrane over the storage chamber.

6.3.2.1 Membrane Theory

The pressure produced from the membrane due to its deflection was analyzed using an equation developed by Senturia [14]. The response of this curve could then be used to infer the effect of volume fluctuations on the applied pressure. Assuming a linear elastic membrane, the equation in the model is derived using energy methods to account for the work done by the external pressure as well as the internal potential energy. The pressure to deflection relationship, denoted by P and w respectively, is shown in Equation (7).

$$P = \left[C_1 \frac{\sigma_0 t}{a^2} + C_b \frac{t^3}{a^4} \frac{E}{(1-\nu^2)} \right] w + C_2 f(\nu) \left[\frac{t}{a^4} \frac{E}{(1-\nu)} \right] w^3 \qquad (7)$$

There are three contributing terms, a linear stiffness term due to the residual stress, σ_0, a second linear stiffness term due to bending, and a cubic stiffness term due to stretching. The dimensions of the membrane are taken into account in the thickness variable t, and in the membrane radius, a. Intrinsic material properties of the membrane include the

Young's modulus, E, and the Poisson ratio, v. The function *f(v)*, is a function of the Poisson ratio, and is dependent on the trial solution used to obtain the equation.

$$w = \frac{c_1}{4}\left[1+\cos\left(\frac{2\pi x}{a}\right)\right]\left[1+\cos\left(\frac{2\pi x}{a}\right)\right] \tag{8}$$

In deriving equation (7), Senturia uses the cosine trial function in equation (8). The *f(v)* value, as well as the finite element model derived constants C_1 and C_2 were taken from Table (1), compiled by Nakladal et al. at Dresden University of Technology [15]. Note that the values in the table depend on the shape of the membrane, be it circular or square.

Shape	C_1	C_2	*f(v)*	Source
Circular	4.0	2.67	$(1.026+0.233\ v)^{-1}$	[16]
	4	2.67	$1-0.24\ v$	[17]
Square	3.41	1.37	$1.446-0.427\ v$	[16]
	3.4	1	$(0.800+.062\ v)^{-3}$	[17]

Table 1: Constants from bulge tests [15].

The value of the constant C_b is not significantly large enough to overcome the bending term's cubic dependence on thickness, which in the case of this application was less than 500 μm. The bending term was therefore ignored in the equation.

6.3.2.2 Membrane Experiments

In order to plot the theoretical curves for the pressure to deflection relationship, values for the material properties were needed. Using linear and cubic fits of the data from bulge test experiments, these constant values could be extracted for the PDMS material used. PDMS membranes were fabricated using double-side polished silicon wafers. Thin layers of silicon dioxide and a masking layer of silicon nitride were deposited on both sides of the wafer. Circles ranging from 1 to 9 mm were patterned on

the wafer surface using a plasma etch to remove unwanted oxide and nitride. Holes were then etched completely through the wafer using KOH etchant with a layer of isopropyl alcohol. By reducing in-plane anisotropy of the etch, the alcohol layer produces straight walls in the holes resulting in round membranes. The nitride acted as an etch stop once the wafer had been etch through. PDMS was spun onto the thin silicon nitride/dioxide membranes remaining over the etched holes. The specific thickness of the PDMS was controlled by the spin rate and time [18]. The experimentation for calibrating these thicknesses is described in Appendix C. After curing, the nitride and oxide remaining in the holes were etched away in a plasma etch. The wafer was then diced to produce individual membranes supported by the remaining silicon wafer sections.

Bill Benett of the LLNL Microtechnology Center designed a test apparatus to hold the individual membranes while allowing deflection measurements under applied pressures. A simple valving setup was devised to allow time for accurate deflection measurement with each step increase in the pressure. The deflection measurements were taken by focusing a microscope on the center of the membrane as it deflected, then recording the corresponding change in height. Pressure measurements were initially taken using a standard pressure valve with 1 psi precision. In order to provide even more precise pressure measurements, a simple water filled manometer was devised which provided measurement to .01 psi. In this manner, data was taken on circular membranes having various thicknesses and diameters.

The low-pressure data from the manometer and the high-pressure data from the pressure gauge were combined to produce the curve in Figure 6.12. The theoretical data

was plotted on this graph using material values of E=.75 MPa, ν=.5, and $\sigma_{0=}$.1 MPa, all values typical for PDMS membranes [19].

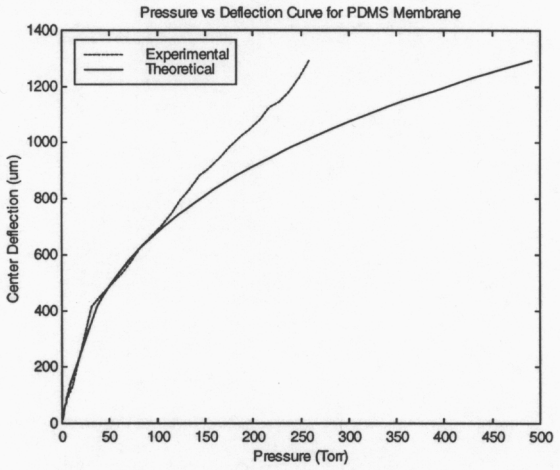

Figure 6.12: Experimental membrane deflections under applied pressure.

Jones et al. also described a similar test done on PDMS membranes for use in valves. Their results, shown in Figure 6.13, revealed results very similar to those in Figure 6.12, and included a scientific explanation for the diversion of the experimental data.

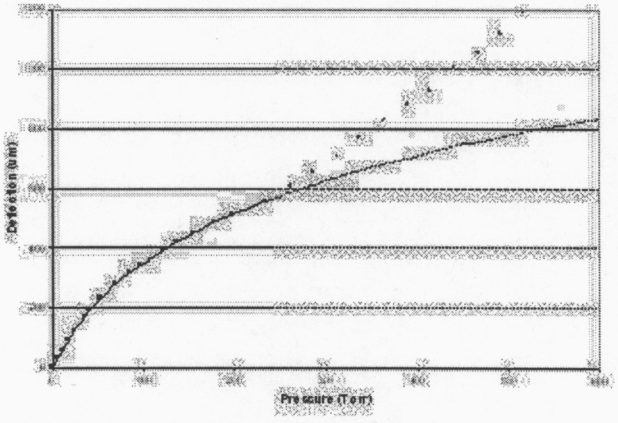

Figure 6.13: Membrane deflection curve under applied pressure adapted from literature [19].

They concluded that a shift from the linear elastic regime to a nonlinear elastic regime caused the experimental data to no longer follow its cubic path.

The data and knowledge obtained from the membrane experiments were integrated into the design for a membrane over the storage chamber. In order to evaluate the effect of decreasing volume in the chamber on the pressure produced by the membrane, the axes of the plot were reversed. The desired form response was one in which the pressure reached a plateau as the deflection continued to increase (Figure 6.14 – Right). If the membrane behaved in this manner, then large volume losses in the storage chamber would have a very minimal effect on the pressure in the system. This was not the observed result though, as the stretching induced cubic stiffness in equation (7) from section 6.3.2.1 tended to dominate the response (Figure 6.14 – Left).

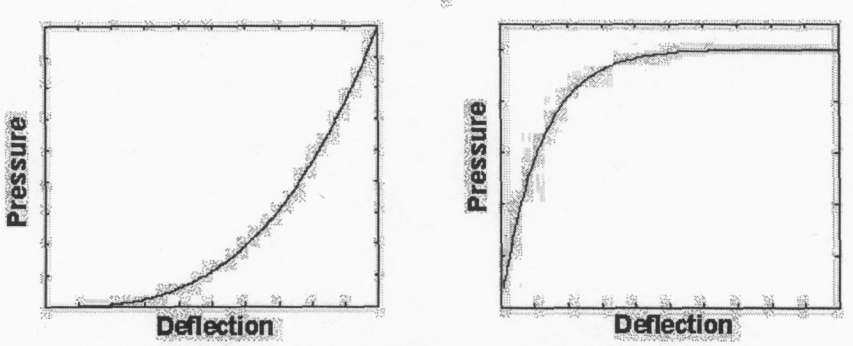

Figure 6.14: Actual and desired pressure vs. deflection curves. Left: Actual theoretical curve with the expected cubic relation between pressure and deflection. Right: Desired curve with a pressure plateau for a large range of deflections.

Still the initial linear range of the deflection, again from equation (7) in section 6.3.2.1, was promising for providing the small changes in pressure change despite the volume changes. By altering the diameter and/or thickness of a membrane in the model, a viable range of relatively flat-sloped curves was found. The shaded region in Figure 6.15 helps discern which of these curves fall in the appropriate membrane displacement and pressure ranges. Using this method it was determined that a 5 mm diameter membrane needed to be approximately 50 μm thick in order to have a shallow enough slope in the designated

ranges. Using the data from experimentation it was found that these dimensions would elicit a nonlinear elastic response well before reaching the desired pressures. Because of this, the membranes were not feasible for use as pressure storage elements in the original means anticipated. Instead, thicker films were used to replace the glass over the storage element because of its bonding properties and an external pressure control system was introduced.

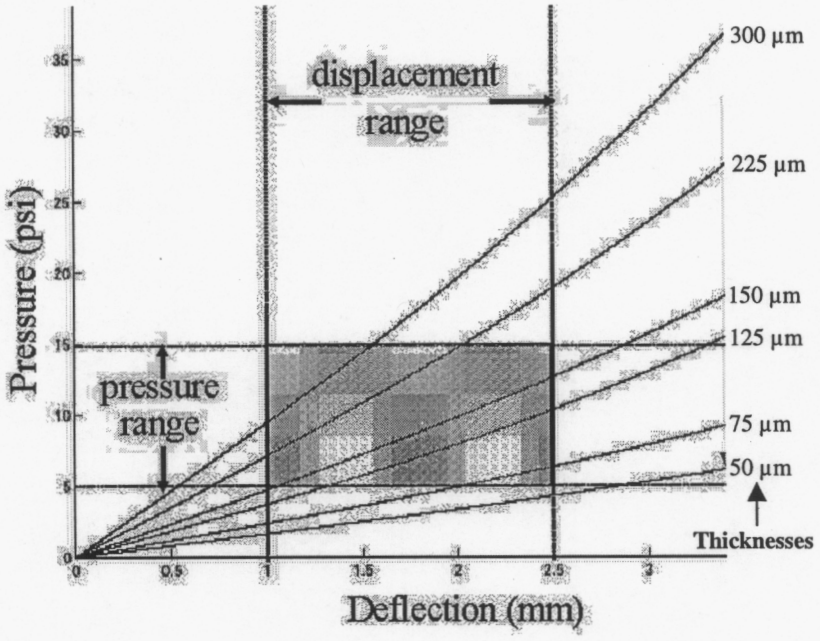

Figure 6.15: Pressure vs. deflection curves through desired ranges. The shaded region represents a specified operating pressure deflection range.

7 Second Generation Fabrication

The second-generation device fabrication did not require the extensive iterations that had been necessary to create a working first generation device. This was due to the process modifications and the design changes made after fabricating the initial devices, and the ample experimentation and modeling integrated into the device design. The most significant process change was the inclusion of a molded alignment feature to facilitate the critical placement of the injector orifice to the electrodes. Fabricating the alignment features required that two substrates – the mold and the actual device - be patterned in nearly identical fashion in order to assure that the features coincided. After patterning features onto a glass substrate for the mold, the substrate was diced and the glass was placed in an acrylic mold in order to cast the desired features into the PDMS. For each step in the process flow, both the mold and device fabrication is included. The complete process flow for both the mold and device is included in Appendix B.

7.1 Substrate

The substrate chosen for both the mold insert and the device was the same BOROFLOAT® glass used in the first generation. The substrates were cleaned and dehydrated to ensure adhesion of the resist during the photolithography steps.

7.2 Electrodes

The array of electrodes described in sections 6.2.1 and 6.2.2 were patterned onto both substrates using the lift off process as before. The device substrate required the

electrodes to facilitate the dielectrophoretic movement of droplets injected into the PFP chamber. The mold substrate was also patterned with the electrodes due to alignment issues. Included on the electrode mask were crosshairs that could be patterned onto the substrate then located with a mask aligner. The other masks used for patterning in the process had similar crosshair features. With the substrate and mask in the aligner the alignment marks could be matched to place the mask. Without alignment features on the substrate, no visible features would exist for aligning because SU-8 features patterned in subsequent steps are transparent.

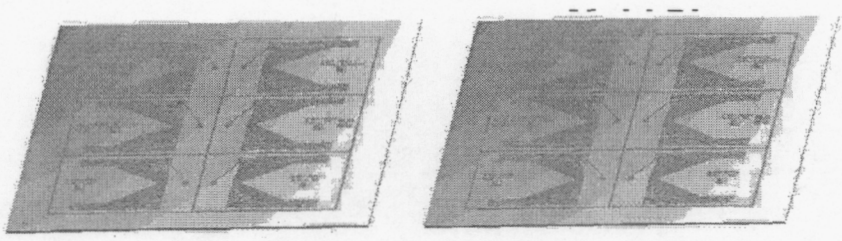

Figure 7.1: Model of the electrodes patterned on both substrates

7.3 Injectors

A molding process was used to create the fluidic injector channels in the PDMS structure before it was bonded to the glass substrate. The injector mold feature was a tapered design with an initial width of 100 μm, tapering to 4, 7, or 12 μm over 4.49 mm, and concluding with a 100 μm long section with parallel walls. These injector features were only required on the mold substrate and not on the actual device substrate.

In order to promote adhesion of the extremely thin sections of SU-8, a 200 angstrom titanium layer was evaporated onto the glass surface. The injectors were

formed using high aspect ratio SU-8 patterned on the mold substrate surface. The SU-8 was spun on the surface at a prescribed rate to obtain the desired thickness (Appendix D). Heights of 4, 7, and 12 μm were needed for the injectors, requiring separate substrates and small changes in each step of the SU-8 process. The SU-8 was baked on a hotplate to solidify the resist then exposed through the photomask to pattern the desired regions. A post exposure bake was required to ensure the cross linking of all exposed areas in the SU-8 layer. A developer provided by the manufacturer was used to wash away all unexposed resist. The parts were then hard-baked in a 120 °C oven to fully cure the resist. (Data from Microchem Corporation is included in Appendices D and E for reference)

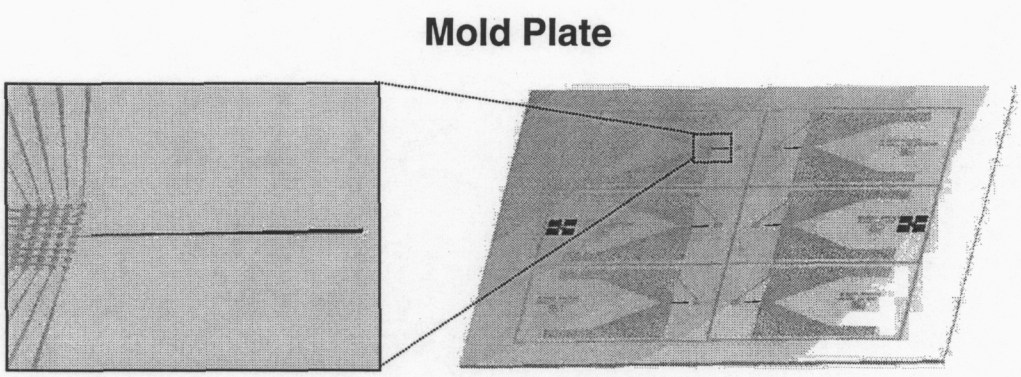

Figure 7.2: Patterned SU-8 injectors on the mold substrate surface.

7.4 Alignment Posts

In order to precisely align the PDMS imprinted injector to the electrodes already patterned on the glass substrate, a single alignment feature was used. The feature was a simple oval shape, patterned 50-90 μm thick in the same location on the mold substrate and device substrate. This way, when the feature was molded into the PDMS structure,

the imprint would be slightly smaller than the feature on the device substrate. When the PDMS was bonded to the device substrate, the molded alignment feature would lock into the impression in the polymer, and the PDMS would be aligned. This process is illustrated in Figure 7.3. The alignment feature was placed near the injector to ensure exact alignment despite any shrinkage during molding. The injector region was the only area which required a precise alignment on the device.

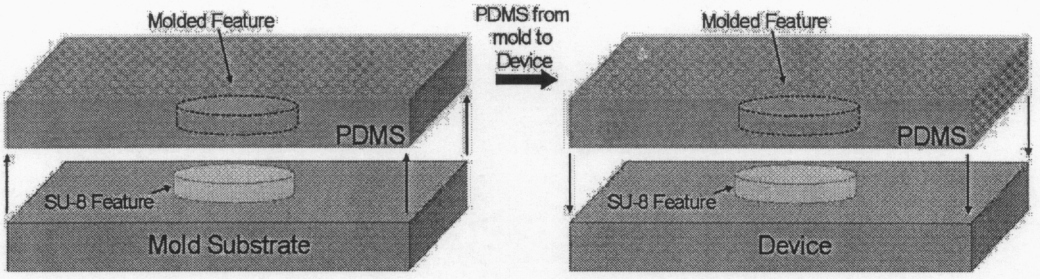

Figure 7.3: Alignment technique using SU-8 feature to define molded feature and a similar feature to aid in alignment on the device.

The alignment features were fabricated using the same techniques as the injector mold had been. The variation in the process being that the thicker alignment features were formed with SU-8 2050 (MicroChem, Newton, MA) spun directly over the previously patterned SU-8 injector. The thicker resist requires longer bake times to solidify the resist, greater exposure doses, and longer to develop the exposed regions. The full data for the thicker resist is included in Appendix E and an example of the alignment feature with respect to the injector is shown in Figure 7.4.

Since the glass mold plates were intended to be placed into an acrylic mold similar to that used in the first generation, there was no means of attaching the PFP and storage chamber mold inserts to the glass. Because of this, the inserts were attached to only the top acrylic layer and designed to have only a thin .02" edge come in contact with the glass. To aid in sealing these inserts to the glass to form precise chamber boundaries,

another layer of SU-8 was patterned onto the surface. This layer included features that replicated the cross section of the rectangular PFP chamber and circular storage chamber. The SU-8 was patterned to 50 μm thick in precisely the same manner as the alignment features. This layer came in direct contact with the injector mold feature so it was necessary to pattern these taller features in this order.

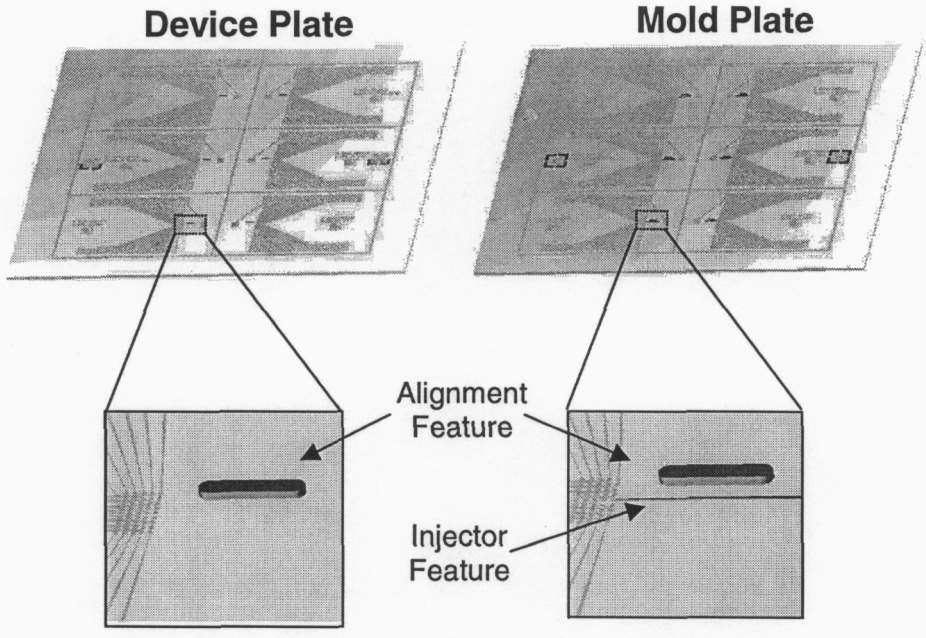

Figure 7.4: Identical alignment features on the device and mold substrates.

7.5 Dice Plates

The mold and device substrates onto which the electrodes and SU-8 features were patterned consisted of six individual sections with slight variations on each to accomplish the experiments desired by MD Anderson. In order to get individual devices and mold inserts it was necessary to dice the plates. This was done using a dicing saw to perform exact cuts along the boundaries patterned during the lift-off process. The glass and

adhered SU-8 features were coated with a polymer resist to create a sacrificial protection layer against the glass particles from the cut. After cutting, the resist was removed in acetone and the parts were cleaned in isopropyl alcohol to ensure a contaminate free surface as in Figure 7.5.

Figure 7.5: Diced device and mold substrates.

7.6 Molding PDMS

The mold plate with the SU-8 alignment, sealing, and injector features was placed into a tightly fit pocket milled from the bottom layer of the acrylic mold as in Figure 7.6. The middle acrylic layer, containing the features for the bulk dimensions, was screwed down onto the bottom layer containing the glass. Delrin inserts forming the PFP and storage chambers were attached to the top acrylic layer with screws as well. Teflon tubing was placed through hollow metal pins and inserted into holes in the storage chamber insert for molding the inlet and outlet fluid channels. The metal pins were inserted into the middle acrylic layer and the mold was assembled.

The mold was injected with polymer precursor, and baked at 66 °C for one hour to cure the PDMS. Upon removal from the mold, the region of the polymer having been in

contact with the SU-8 photoresist was rinsed with acetone and isopropyl alcohol. This molding process was performed by Julie Hamilton of the LLNL Microtechnology Center.

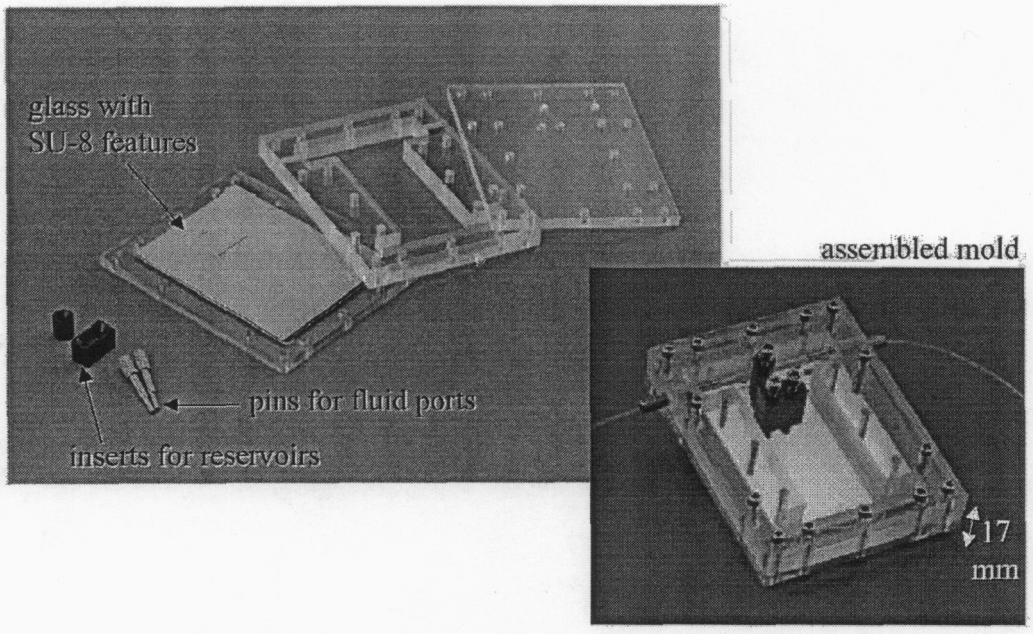

Figure 7.6: Unassembled and assembled view of acrylic mold with glass mold insert. The fluid reservoirs are formed by delrin inserts. The inlet and outlet port are formed with hollow pins, through which Teflon tubing is inserted and connected to the cylindrical insert.

7.7 Bonding

To bond the molded PDMS to the glass substrate containing the electrodes, the bonding surfaces were exposed to an oxygen plasma then immersed in methanol to provide time for alignment before the parts bonded. Using a microscope for visual reference, the protruding alignment feature on the substrate was inserted in the cavity in the PDMS formed by the features replica on the mold. The methanol was evaporated by

placing the glass directly onto a hotplate, creating a permanent bond between the two materials. This bonded device is illusrated in Figure 7.7.

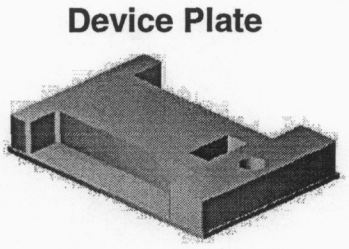

Figure 7.7: Model of the molded PDMS bonded to the device substrate.

7.8 Capping

Sealing the storage chamber was necessary to accumulate the pressures to form droplets from the injectors and to force these droplets beyond the geometrical threshold at which they would release spontaneously. This seal was made using a simple glass rectangle of the appropriate dimensions to cover the storage chamber. Similar to the previous bonding processes, the glass and PDMS surface were rinsed with ethanol to remove all contaminants and placed in an oxygen plasma for one minute. The glass was then pressed into position to form the irreversible bond over the chamber. Thick layers of PDMS could also be used to provide the same pressures with greater bond strength.

7.9 Surface Coating

With the microfluidic features bonded to the electrode's substrate, a passivation layer over the electrodes was still necessary. The vapor-deposited polymer, parylene, had

been chosen as the appropriate material for providing separation between the electrodes and droplets and for creating a hydrophobic surface in the PFP chamber. The injector channel had been oversized by 1 μm on all sides to accommodate a parylene coating of this thickness. The injector channel was coated to provide a consistent contact angle on all four walls. An appropriate amount of parylene for a 1 μm surface coating was placed in the diffusion chamber and allowed to disperse onto the device.

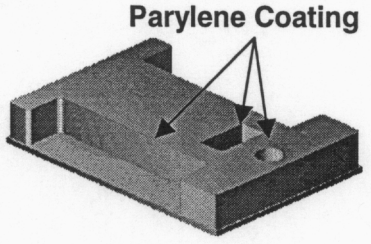

Figure 7.8: Model of a device after coating with parylene film.

8 Second Generation Results

The second-generation device fabrication was enhanced by the design and process refinements made to first generation device. Several improvements over the first generation device were made, laying the foundation for a final design in which the electronics would be integrated with the microfluidics. For the hybridized second generation, nearly all of the desired attributes had been successfully incorporated in the device.

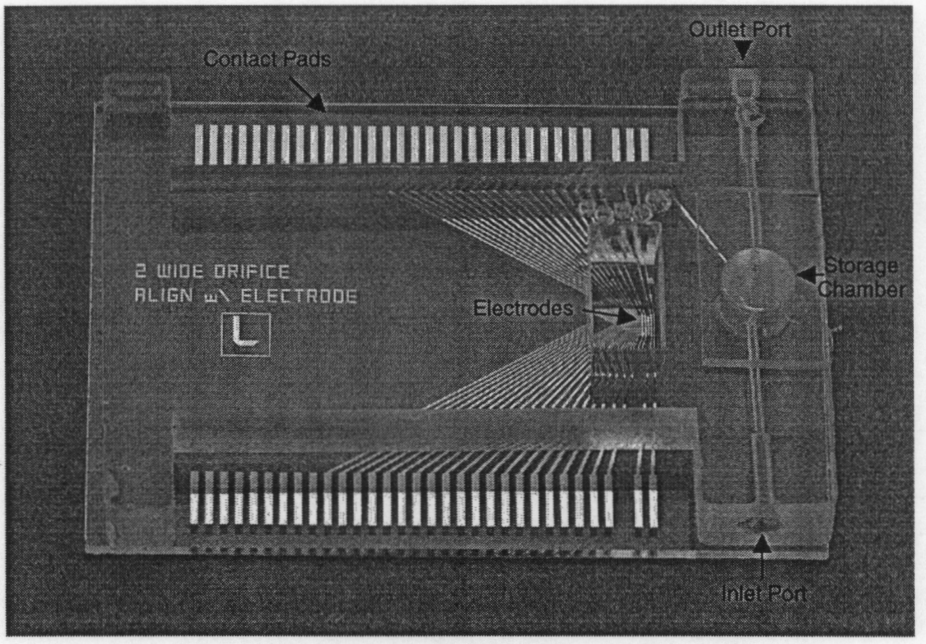

Figure 8.1: Example of a completed second generation device.

A final iteration of inspection by LLNL and testing by MD Anderson was necessary in order to discern any remaining difficulties in the device design. This information would be used for designing a final generation integrated device.

8.1 Electrodes

The new shortened and tapered design for the electrodes was successful in minimizing the effect of contaminants during fabrication. The new dimensions allowed for small breaks in the patterned conductors without completely disrupting the electrical pathway. Addition of the grounding pad beneath the storage chamber provided the ability to control the charge on the fluid before injected into the chamber.

8.2 Injector and Chamber Features

In order for the injector orifice to have the desired hydraulic diameter, the results from the SU-8 fabrication were investigated.

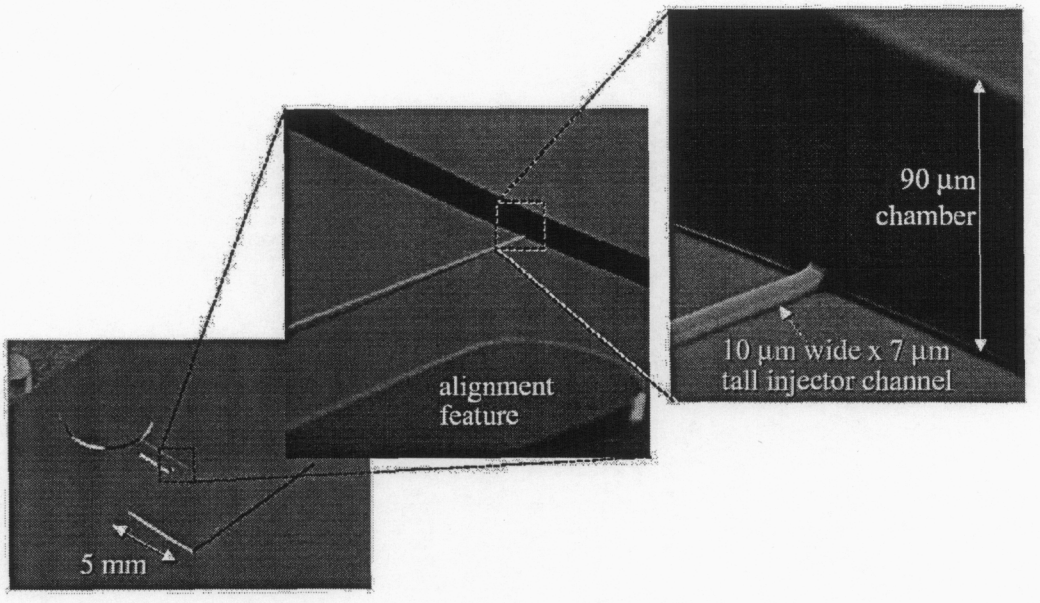

Figure 8.2: SEM pictures of the injector mold and adjacent PFP chamber mold.

Figure 8.2 displays a series of views of the injector feature as well as the intersection between the injector feature and the PFP chamber feature. These SEM pictures reveal a

well-defined square section in the injector feature mold as well as an adequate intersection at its tip. The desired intersection would be a perfect square so the slight curvature from the surface tension during fabrication may adversely affect the droplet ejection. Some control may be lost over the final radius of droplets as they are ejected from the channels.

The corresponding molded injector channel in the completed device was also viewed in the SEM. Two important resulting characteristics are evident in Figure 8.3 below.

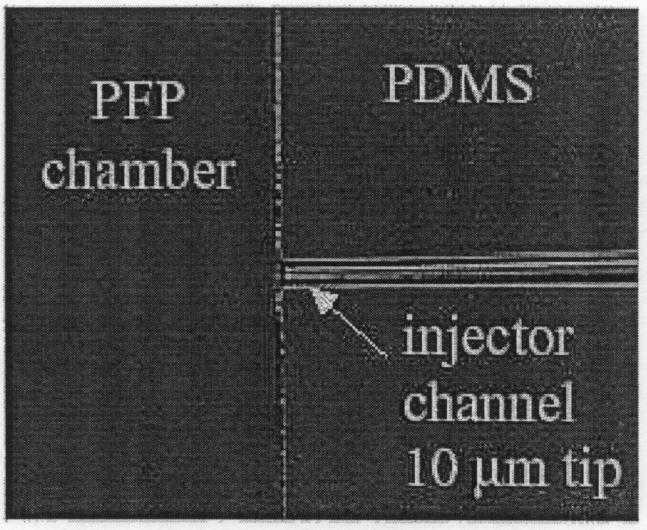

Figure 8.3: Zoomed view of the orifice of an injector and the edge of the PFP chamber.

The injection channel is very well formed, with a very defined orifice for ejecting droplets. The edge of the PFP chamber is also very straight and well defined as well. If the edge were not well defined it could disrupt the shape of droplets during ejection do. The molding technique utilized in the injector channel fabrication proved to be very precise.

8.3 Alignment

Alignment of the electrodes to the microfluidics was required to be within a narrow 20 μm range in two dimensions. To ensure this accuracy, the mold substrate used for creating the microfluidics was inspected before placing it in the acrylic mold. The electrodes in Figure 8.4 were patterned onto the mold surface due to their inclusion on the mask used for alignment features. In Figure 8.4 they provide a means of evaluating the mold features placements.

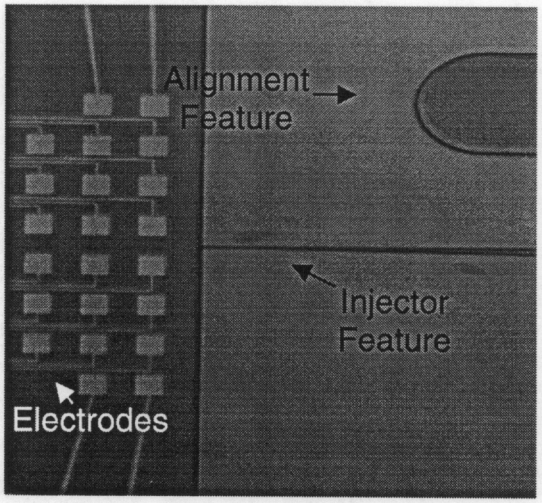

Figure 8.4: SU-8 alignment feature and injection feature patterned at a precise distance relative to the electrodes on the mold.

Qualitatively, the alignment of the injector tip to the electrodes appeared to be very accurate. The tip was supposed to split the distant between the two center electrodes, as it appears to in Figure 8.4. The vertical placement should be the same distance as the width of one electrode. This position also appears to be very good from a qualitative perspective. With good alignment on the mold, it was expected that the features molded from this substrate would also produce very accurate alignment.

The alignment between the electrodes did not transfer well to the molded device in some devices. The image in Figure 8.5 shows that faint channel misaligned from the center of the electrodes by approximately 50 μm. This was likely due to a compilation of minor misalignments in the injector feature creation, mold feature creation, or when the mold substrate was aligned in the acrylic mold. This alignment could be readjusted by using a mask aligner during the photolithography processes to ensure exact overlap of the features.

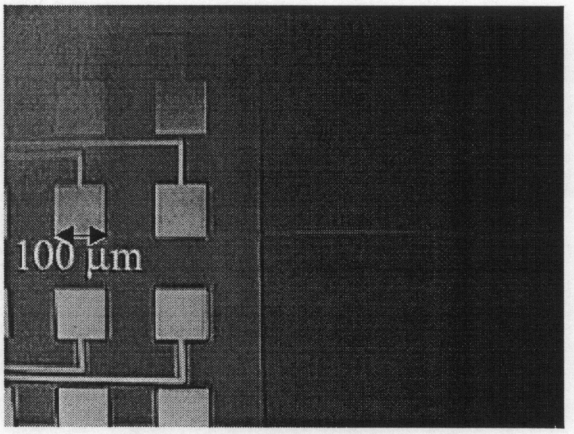

Figure 8.5: Microscope view of the injector orifice and electrodes on a bonded device.

A second factor in misalignment was the premature evaporation of methanol used to delay bonding. This problem can be addressed by adding additional methanol to the interface before mating the substrate and PDMS.

8.4 Droplets

Testing of the microfluidics portion revealed that droplet formation was controllable with pressures in the anticipated range. The tapered channel significantly reduced the fill pressures to an acceptable range. The hydrophobic surface coating in the

channel and on the PFP surface created the desired contact angle to maintain spherical droplets in an air or bromododecane medium. Droplets injected from micropipettes tended to continue expanding without the application of a DEP force. In the second generation device, these droplets were injected using only pressure injection. This was probably due to the rectangular dimensions "pinching off" the droplets in the devices.

9 Conclusion

Design of the first generation used the extensive research from MD Anderson to develop a microfluidic system for injecting droplets onto an array of electrodes. Initial fabrication of this system was intended to use planar etching or molding techniques to pattern the fluid injection channels out of PDMS polymer. Due to a slow etch rate of only .5 μm/min, coupled with rapid contamination of the reactive ion etcher used for patterning the polymer this approach was unsuccessful. Patterning PDMS using a planar molding technique with removal of photoresist features was not achievable due to thin layers of polymer over the resist. A micromolding technique was therefore instituted using finely patterned features in SU-8 to pattern the injector channel.

The second generation device design and fabrication utilized the successful micromolding from the first generation and improved upon it by adding alignment features for accurately positioning the injector with respect to surface electrodes. Modeling of the fluid system provided an optimized design for the injector which tapered in two dimensions to avoid clogging and reduce pressures. A fluid capacitor for maintaining pressure levels during droplet injection was also modeled and experimented with but did not prove feasible for the device. The second generation device proved capable of creating well defined droplets in the PFP chamber with relatively low pressures.

By creating non-integrated devices in the first two generations, the microfluidic design and fabrication were able to rapidly advance without being restricted by associated electronics. Had the device been initially integrated, compatibility problems with the

microfluidic fabrication could have severely hampered the project. Instead, both groups were able to continually design and test their components with multiple iterations without interfering with the progress of the other components. The use of compatible materials and processes in the PDMS fabrication is expected to make integration of the microfluidics and microelectronics a trivial matter.

Once integrated, with the microfluidic system bonded directly to the microelectronics, the device will be able to perform a variety of assays in the PFP chamber by injecting various chemicals from the multiple storage wells. The integrated circuits and software will allow for control of the solutions injected into the PFP chamber as well as the fluids injected into the chamber. This analysis flexibility should provide extensive applications for the device in chemical detection, synthesis, and manipulation.

10 Future Work

In the final device, illustrated in Figure 10.1, the electrodes for dielectrophoresis and the addressing high voltage electronics will be fabricated onto a silicon wafer. The microfluidics will be molded from PDMS, using a method similar to the second generation, and bonded to the silicon wafer. The transition to a silicon wafer should be facilitated by the use of glass in the previous devices. The bonding properties of silicon and glass to PDMS are nearly identical, so the change should not affect adherence of the microfluidics.

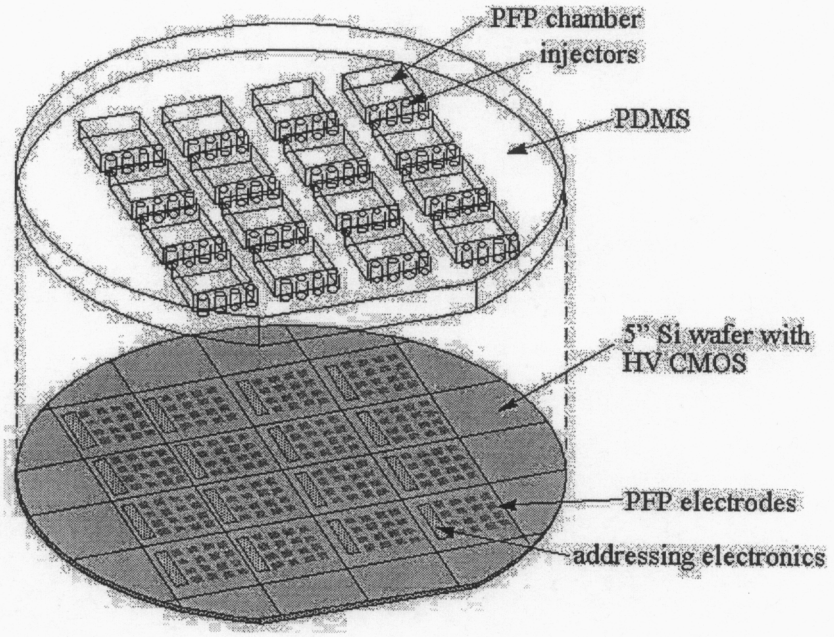

Figure 10.1: Intended design for the integrated PFP device with the integrated circuits patterned in a silicon wafer, and the microfluidics patterned in PDMS.

The addition of multiple storage chambers and connecting injector channels should only require a modification to the acrylic mold and inserts. The transition to a multiple device process should not be difficult using the refined techniques from the second generation, as it requires only an expansion of the current design.

The possible difficulties in creating a final device lie in the interaction of the microelectronic materials and the chemicals used for microfluidic fabrication. In order to fabricate alignment features on the surface of the silicon wafer, SU-8 processing is needed. This includes exposure to high temperatures, UV light, and a solvent based developer. If these conditions do not affect the underlying microelectronics on the silicon wafer, then a direct transferal of the fabrication techniques is possible. Otherwise, further modification will be necessary.

11 References

[1] Vykoukal, J., Schwartz, J., Becker, F. and Gascoyne, P. "A programmable dielectrophoretic fluid processor for droplet-based chemistry" in in *Micro Total Analysis Systems 2001*, A. van den Berg et al. (eds) (Kluwer Academic Publishers, The Netherlands, 2001), pp 72-74.

[2] Krihak, Michael. "BioFlips". DARPA MTO Core Technology Areas. http://www.darpa.mil/mto/bioflips/index.html (24 April 2002)

[3] Duffy D.C., McDonald J.C., Schueller O.J.A., Whitesides G.M. "Rapid Prototyping of Microfluidic Systems in Poly(Dimethylsiloxane)" ANAL CHEM 70 (23): 4974-4984 DEC 1 1998

[4] Yang, J., Vykoukal, J., Noshari, J., Becker, F., Gascoyne, P., Krulevitch, P., Fuller, C., Ackler, H., Hamilton, J., Boser, B., Eldredge, A., Hitchens, D. and Andrews, C. "Dielectrophoresis-based Microfluidic Separation and Detection Systems", INT. J. ADV. MANUFACTURING SYSTEMS 3(2):1-12, 2000

[5] Wang, X.-J., Wang, X-B., Becker, F.F., Gascoyne, P.R.C. "A Theoretical Method of Electrical Field Analysis for Dielectrophoretic Electrode Arrays Using Green's Theorem". J. PHYS. D: APPL. PHYS. 29:1649-1660, 1996.

[6] Wang, X-B., Huang, Y., Becker, F.F., and Gascoyne, P.R.C. "A Unified Theory of Dielectrophoresis and Travelling Wave Dielectrophoresis". J. PHYS. D: APPL. PHYS., 27:1571-1574, 1994.

[7] Gascoyne P., Krulevitch P., Hitchens D., Gilbert J., Current W., "A General-Purpose Analysis System Based on a Programmable Fluid Processor". Presentation for DARPA BioFLIPS PI Meeting. September, 2002

[8] Schwartz, Jon A., "Dielectrophoretic Approaches to Sample Preparation and Analysis", Doctoral Dissertation, University of Texas Graduate School of Biomedical Sciences, 2001.

[9] Schott Corporation Technical Glass Division. "BOROFLOAT® Borosilicate Float Glass". http://www.us.schott.com/tgd/english/products/boromenu.html (24 April 2002)

[10] Duffy DC, Jackman RJ, Vaeth KM, et al. "Patterning Electroluminescent Materials with Feature Sizes as Small as 5 μm Using Elastomeric Membranes as Masks for Dry Lift-off". ADV MATER 11 (7): 546-+ MAY 7 1999

[11] Jo BH, Van Lerberghe LM, Motsegood KM. "Three-dimensional Micro-channel Fabrication in Polydimethylsiloxane Elastomer" J MICROELECTROMECHS 9 (1): 76-81 MAR 2000

[12] Homma H., Lee C. R., Kuroyagi T., Izumi K. "Evaluation of Short Time Variation of Hydrophobicity of Silicone Rubber Using Dynamic Contact-angle Measurement" Report from Central Research Institute of Electric Power Industry. Nagasaki Japan

[13] Humphrey B. "Vapor Phase Consolidation of Books with the Parylene Polymers". J AMERICAN INSTITUTE CONSERVATION. 25 (1): 15-29 1986

[14] Senturia S., "Microsystem Design". Boston, MA: Kluwer Academin Publishers, 2001 pp257-260

[15] Nakladal A., Buchhold R., Kohler R., Gerlach G., Stavrev M., Wenzel C., Baumann K., Nowak B., "Bulge Test Investigation of the Influence of Moisture on Mechanical Properties in Thin Polymer Layers". MATERIALS RESEARCH SOCIETY SYMP., Materials Research Society 518: 105-110 1998

[16] Lin P., Senturia S. "The In-situ Measurement of Biaxial Modulus and Residual Stress of Multilayer Polymer". MATERIALS RESEARCH SOCIETY SYMP., Materials Research Society 227: 41-46 1990

[17] Small M., Vlassak J., Powell S. "Accuracy and Reliability of Bulge Test Experiments". MATERIALS RESEARCH SOCIETY SYMP., Materials Research Society 308: 159-164 1993

[18] Maghribi M., Hamilton J., Polla D., Rose K., Wilson T., Krulevitch P., "Stretchable Micro-electrode Array". Submited to IEEE for publication. March 2002

[19] Yang X., Grosjean C., Tai Y.C. "Design, Fabrication, and Testing of Micromachined Silicone Rubber Membrane Valves". J MICROELECTROMECHS 8 (4): 393-402 DEC 1999

[20] Microchem Products. "SU-8 Resists". http://microchem.com/products/su_eight.htm (1 May 2002)

12 Acknowledgements

This work was performed under the auspices of the U. S. Department of Energy by the University of California, Lawrence Livermore National Laboratory under Contract No. W-7405-Eng-48.

Research was carried out at the Lawrence Livermore National Laboratory Center for Microtechnology as a student guest while enrolled at the Massachusetts Institute of Technology in the Engineering Internship Program

Development of a the Programmable Fluidic Processor is a collaborative effort between MD Anderson and the Lawrence Livermore National Laboratory Center for Microtechnology, with assistance from University of California at Davis, Coventor, and Lynntech Inc. The project is funded through the Defense Advanced Research Project Agency's Biological Fluidic Chips program.

The research team at MD Anderson is responsible for the PFP device. They provided a plethora of knowledge regarding dielectrophoresis as well as multiple models of the phenomenon from Coventor. Their research and experimentation on dielectrophoresis and droplet ejection were integral to the formulation of appropriate designs for the devices described within this thesis. They were also responsible for testing of completed devices and provided feedback for subsequent device generations. Peter Gascoyne, Jody Vykoukal, and Jon Schwartz were the primary collaborators with the author and their assistance is greatly appreciated.

Chuck McConaghy of the LLNL Microtechnology and Professor Wayne Current from the University of California at Davis developed the microelectronics for the PFP device. This was a parallel project with the microfluidic system development with a merge of the projects to occur in the final integrated device.

This research would not have been possible without the help of the project team at the LLNL Microtechnology. Project leader Peter Krulevitch provided exceptional guidance for this research and for the overall project at LLNL. His ingenuity and experience were extremely beneficial in the design and process flow for the devices. He also provided assistance in analyzing results from the research and in editing. Julie Hamilton provided guidance in the microfabrication of devices and fabricated the second generation device. Bill Benett designed the basic geometry for the devices provided input into appropriate design modifications. He was also responsible for designing the test apparatus for measuring membrane deflections. Mariam Maghribi provided extensive help and information on microfabrication with PDMS and Alex Papavasiliou was repeatedly consulted with regarding modeling of the fluidic system.

A special thank you to Douglas Hart who provided input as advisor at MIT and ensured the progress of the project during his visit to Lawrence Livermore.

Appendix A: First generation process flow

I. Pattern Electrodes (Mask 1)
   1. Prepare glass
      a) Clean 5" glass in 1:1 S_2HO_4/H_2O_2
      b) Dehydrate glass at 120 °C oven for at least one hour
   2. Pattern photoresist
      a) Spin on AZ 4110 photoresist @ 3000 rpm (program 5 on CEE)
      b) Softbake 90 °C for 20 mins
      c) Expose resist for 6 seconds (132 mJ)
      d) Chlorobenzene soak for 2 mins
      e) N_2 dry
      f) Develop resist in AZ Developer 400K @ 1:4 AZ/H_2O for ~80 sec
   3. Evaporate metal in EB3 e-beam
      a) Chrome 200 Å
      b) Gold 1000 Å
   4. Lift off metal and photoresist using acetone

II. Passivate with SiO_2 (Mask 2)
   1. PECVD SiO_2 for 15 minutes (1/2 μm)
   2. Pattern photoresist
      a) Spin on 4620 resist @ 3000 rpm for 20 sec
      b) Softbake for 20 min @ 90 °C
      c) Expose for 60 sec
      d) Develop in 1:1 AZ developer/H_2O for 1.5 min
      e) Hardbake for 30 min @ 90 °C
   3. Etch SiO_2 layer
      a) Etch in RIE using CF4:40 and O2: 10 for 10 min
      b) Check gold pads for resistance to ensure etch depth is sufficient
   4. Strip photoresist using acetone and isopropyl alcohol

III. Pattern photoresist lines (Mask 3)
   1. Spin on 4620 resist to 2 μm or 5 μm
   2. Expose 60 seconds
   3. Develop in 1:1 AZ developer/H_2O

IV. Pattern SU-8 injector nozzles (Mask 4)

V. Remove resist to form channels
   1. Ultrasonic acetone for 5 minutes

VI. Mold PDMS for damming (Mold 1)
   1. Assemble mold
      a) Attach bottom (.125 plate with capcom sheet)
      b) Insert islands and align hole on cylinder

c) Insert tubing and tubing aligner

2. Add PDMS (~6.35 cm^3)
   a) Mix PDMS at 10:1 and degas
   b) Pour PDMS onto mold, and assemble top
   c) Bake at 66 °C for at least 1 hour
3. Bond molded part to glass
   a) Remove .062 plate
   b) Remove .125 plate
   c) Place glass in alignment plate

VII. Transfer cap

VIII. Hydrophobic coating

Appendix B: Process flow for second generation devices

IX. Pattern electrodes (Mask 1)

5. Prepare glass
   c) Clean 5" glass in 1:1 S_2HO_4/H_2O_2
   d) Dehydrate glass at 120 °C for one hour
6. Pattern photoresist
   g) Spin on AZ 4110 photoresist at 3000 rpm
   h) Softbake 90 °C for 20 mins
   i) Expose resist (132 mJ)
   j) Chlorobenzene soak for 2 mins
   k) N_2 dry
   l) Develop resist in 1:4 AZ 400K / H_2O for ~80 sec
7. Evaporate metal in EB3 e-beam
   c) Chrome 200 Å
   d) Gold 1000 Å
8. Lift off metal and photoresist using acetone
   a) Rinse with isopropyl alcohol
   b) N_2 dry

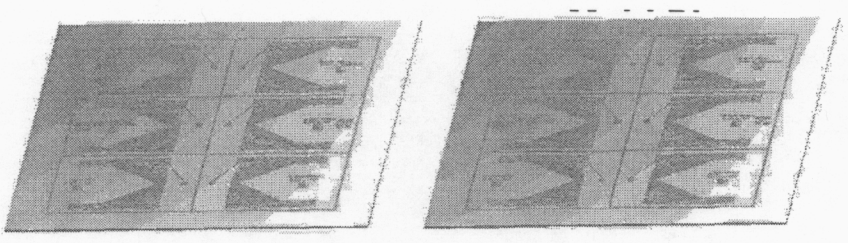

X. Pattern injectors (Mask 2)

For 2 μm tall injector (4 μm of SU-8)

4. Spin on SU-8 2005 at 3600 rpm
5. Soft bake at 65 °C for 60 s then 95 °C for 120 s
6. Expose under 365nm flood source with 120-130 mJ/cm^2
7. Bake at 65 °C for 60 s then 95 °C for 60 s
8. Develop in SU-8 developer for 60 s
9. Hardbake at 120 °C for 30 min

For 5 μm tall injector (7 μm of SU-8)

1. Spin on SU-8 2005 at 2000 rpm
2. Soft bake at 65 °C for 60 s then 95 °C for 120 s
3. Expose under 365nm flood source with 150-180 mJ/cm^2
4. Post exposure bake at 65 °C for 60 s then 95 °C for 60 s
5. Develop in SU-8 developer for 60 s
6. Hardbake at 120 °C for 30 min

For 10 μm tall injector (12 μm of SU-8))

1. Spin on SU-8 2005 at 1200 rpm
2. Soft bake at 65 °C for 60 s then 95 °C for 120 s
3. Expose under 365nm flood source with 185-200 mJ/cm^2
4. Post exposure bake at 65 °C for 60 s then 95 °C for 120 s
5. Develop in SU-8 developer for 120 s
6. Hardbake at 120 °C for 30 min

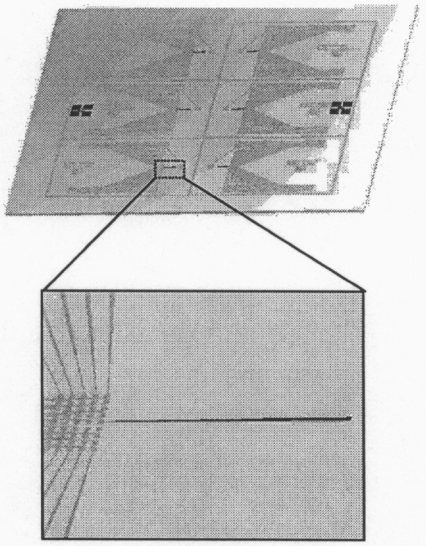

XI. Pattern alignment posts (Mask 3)

For 50 μm tall features

1. Spin on SU-8 2050 at 3000 rpm
2. Soft bake at 65 °C for 3 min then 95 °C for 6 min
3. Expose under 365nm flood source with 400-500 mJ/cm^2
4. Post exposure bake at 65 °C for 1 min then 95 °C for 5 min
5. Develop in SU-8 developer for 6 min

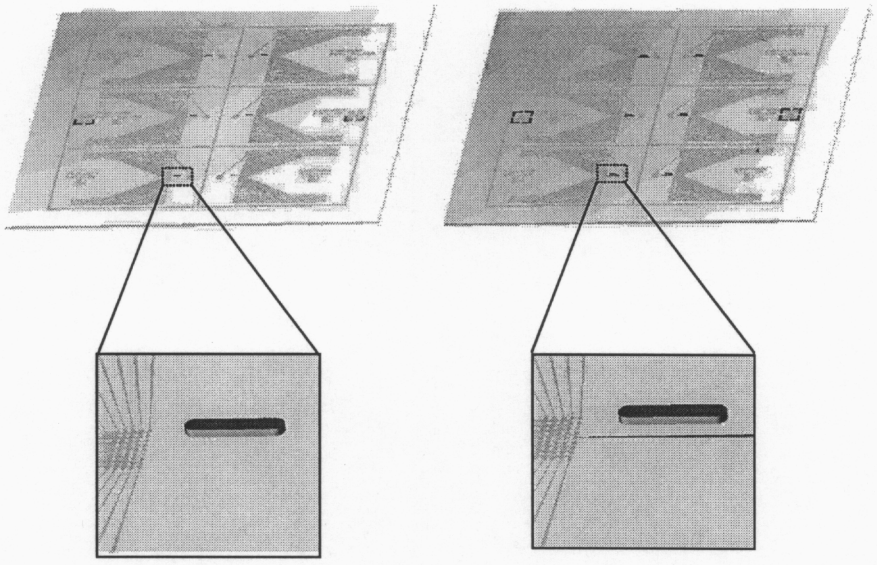

XII. Dice plates

1. Coat with protective layer of photoresist

XIII. Mold PDMS

1. Press glass mold device into alignment plate
2. Assemble acrylic mold
3. Insert teflon tubing and metal pins
4. Prepare PDMS
5. Inject PDMS into mold
6. Cure at 66 °C for 60 mins
7. Disassmeble mold and remove PDMS block

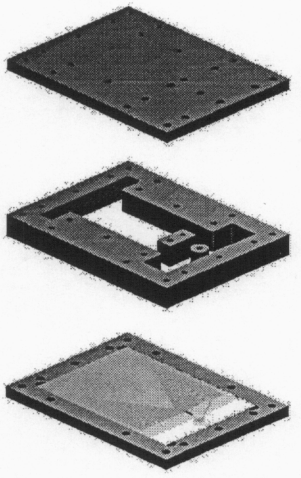

XIV. Bonding

1. Rinse glass device and PDMS block in ethanol
2. Oxygen plasma for 1 min at 100 W
3. Soak in methanol for 5 min
4. Align parts using SU-8 alignment feature
5. Place on 90 °C hotplate for ~10 min. to evaporate methanol

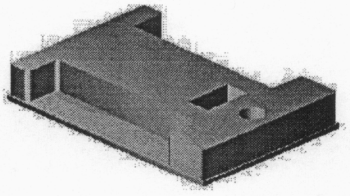

XV. Coating

1. Cover electrode and top layer of PDMS
2. Apply 1 μm thick Parylene coating

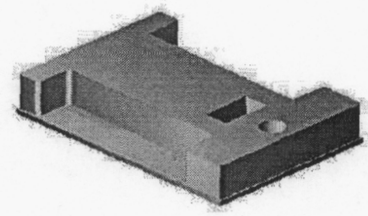

XVI. Membrane

1. Bond on glass or PDMS membrane

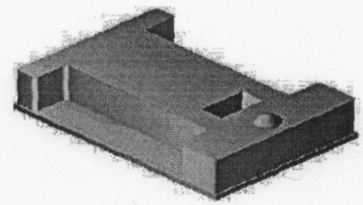

APPENDIX C: Calculation of PDMS spin thicknesses

The following curves were developed by measuring resulting thicknesses from various spin rates [18]. The measurements for two spin times were taken to provide data on this effect as well.

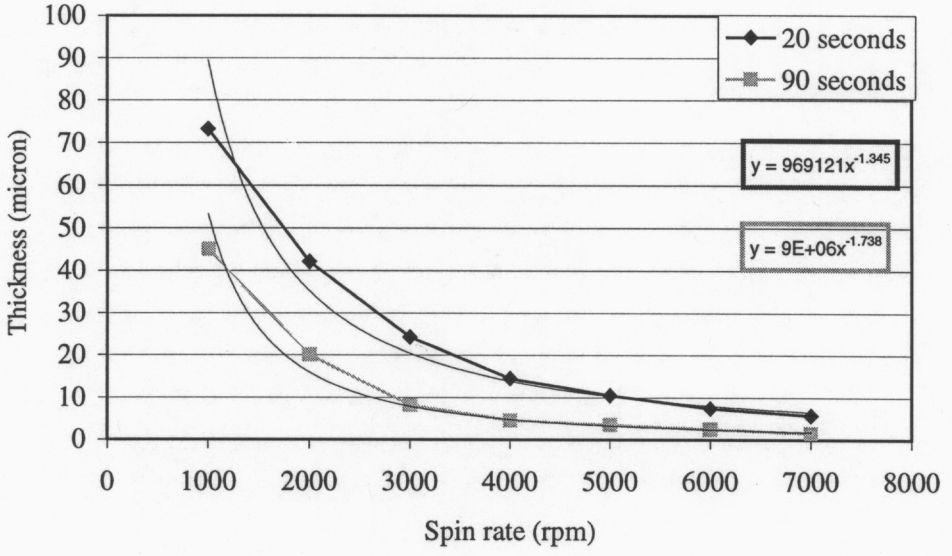

Using a power fit of the data, an approximate equation was generated relating thickness to spin rate. Solving these equations for the spin rate provided an equation for the thickness with variable spin rates. These equations provided a means for producing accurate PDMS film thicknesses during fabrication.

$$Time = 20s \qquad Thickness(\mu m) = \frac{2.82x10^4}{speed(rpm)^{.74}} \tag{1}$$

$$Time = 90s \qquad Thickness(\mu m) = \frac{1.0x10^4}{speed(rpm)^{.58}} \tag{2}$$

Appendix D: SU-8 processing for thickness less than 25 μm [20]

Patterning of SU-8 features with a thickness less than approximately 25 μm requires the use of SU-8 2002, 2005, 2010, or 2015. The processing consists of six major process steps, each listed below for a range of thicknesses. For each process step, Microchem has developed a chart or table to aid in fabricating features of various thicknesses.

1. Wafer Coating

Product	Viscosity **	Thickness	Spin Speed
	cst @ 25°C	μm	rpm
SU-8 2002	43	1.5	3000
		2	2000
		5	1000
SU-8 2005	293	5	3000
		7	2000
		15	1000
SU-8 2010	1050	10	3000
		15	2000
		30	1000
SU-8 2025*			
SU-8 2035*			
SU-8 2050*			
SU-8 2075*			

Table 1. Thickness vs. spin speed data for selected SU-8 2000 resists.

Appropriate thickness values can be determined from either Table 1, or from the chart in Figure 1.

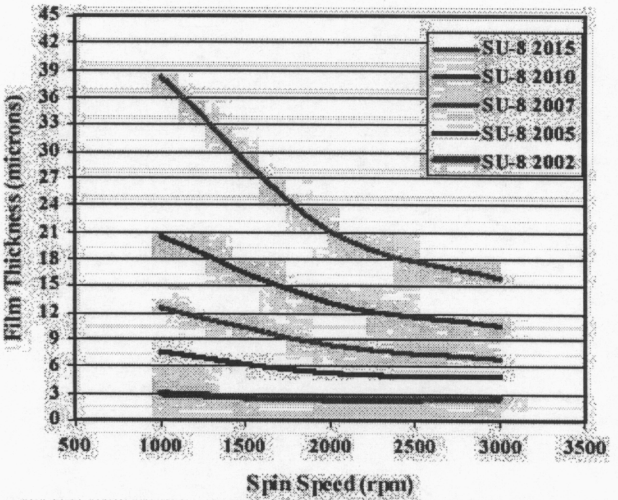

Figure 1. Spin speed vs. thickness curves for selected SU-8 2000 resists.

2. Soft Bake Parameters

Product	Thicknesses	Soft Bake Times	
	µm	STEP 1 65°C	STEP 2 95°C
SU-8 2002	2	60	120
	2.5	60	120
	3	60	120
SU-8 2005	5	60	120
	6	60	120
	7.5	60	120
SU-8 2007	7	60	120
	8.5	60	120
	12.5	60	120
SU-8 2010	10	60	120
	13	60	120
	20	60	180
SU-8 2015	15	60	120
	21	60	180
	38	120	300

Table 2. Recommended soft bake parameters

3. Exposure doses

Product	Thicknesses	Exposure Dose
	µm	mJ/cm^2
SU-8 2002	2	95-115
	2.5	95-115
	3	95-115
SU-8 2005	5	120-130
	6	120-130
	7.5	150-180
SU-8 2007	7	150-180
	8.5	150-180
	12.5	185-200
SU-8 2010	10	185-200
	13	185-200
	20	190-210
SU-8 2015	15	190-210
	21	190-210
	38	220-240

Table 3. Recommended expose dose processes

4. Post Exposure Bake Times

Product	Thicknesses	P.E.B. Times (sec)	
	µm	STEP 1 65°C	STEP 2 95°C
SU-8 2002	2	60	60
	2.5	60	60
	3	60	60
SU-8 2005	5	60	60
	6	60	60
	7.5	60	60
SU-8 2007	7	60	60
	8.5	60	120
	12.5	60	120
SU-8 2010	10	60	120
	13	60	120
	20	60	120
SU-8 2015	15	60	120
	21	60	120
	38	60	180

Table 4. Recommended post expose bake parameters

5. Development Times

Product	Thicknesses	Develop Time
	µm	sec
SU-8 2002	2	60
	2.5	60
	3	60
SU-8 2005	5	60
	6	60
	7.5	60
SU-8 2007	7	60
	8.5	120
	12.5	180
SU-8 2010	10	120
	13	180
	20	180
SU-8 2015	15	180
	21	180
	38	300

Table 5. Recommended develop processes

6. Hard Bake

SU-8 2000 has good mechanical properties, therefore hard bakes are normally not required. For applications where the imaged resist is to be left as part of the final device, the resist may be ramp/step hard baked between 150-200°C on a hot plate or in a convection oven to further cross link the material. Bake times vary based on type of bake process and film thickness.

Appendix E: SU-8 processing for thickness greater than 25 μm [20]

Patterning of SU-8 features with a thicknesses greater than approximately 25 μm requires the use of SU-8 2025, 2035, 2050, or 2075. The processing consists of six major process steps, each listed below for a range of thicknesses. For each process step, Microchem has developed a chart or table to aid in fabricating features of various thicknesses.

2. Wafer Coating

Product	Viscosity	Thicknesses	Spin Speed
	cst @ 25°C	μm	rpm
SU-8 2025	4,800	25	3000
		41	2000
		75	1000
SU-8 2035	7,000	35	3000
		55	2000
		110	1000
SU-8 2050	17,000	50	3000
		75	2000
		165	1000
SU-8 2075	32,000	75	3000
		110	2000
		225	1000

Table 1. Thickness vs. spin speed data for selected SU-8 2000 resists.

Appropriate thickness values can be determined from either Table 1, or from the chart in Figure 1.

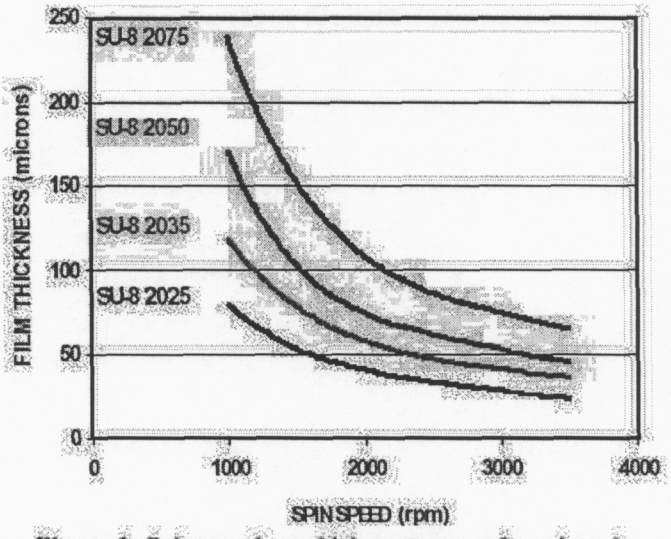

Figure 1. Spin speed vs. thickness curves for selected SU-8 2000 resists.

2. Soft Bake Parameters

Product	Thickneses	Soft Bake Time (min)	
	µm	STEP 1 65°C	STEP 2 95°C
SU-8 2025	25	1	3
	40	2	5
	75	3	9
SU-8 2035	35	2	5
	55	3	6
	110	5	20
SU-8 2050	50	3	6
	75	3	9
	165	5	30
SU-8 2075	75	3	9
	110	5	20
	225	5	45

Table 2. Recommended soft bake parameters

7. Exposure Dose

Product	Thicknesses	Exposure Dose
	µm	mJ/cm^2
SU-8 2025	25	220-240
	40	250-350
	75	500-600
SU-8 2035	35	250-350
	55	400-500
	110	500-650
SU-8 2050	50	400-500
	75	500-600
	165	600-650
SU-8 2075	75	500-600
	110	500-650
	225	625-675

Table 3. Recommended expose dose processes

8. Post Exposure Bake Times

Product	Thicknesses	P.E.B. Time (min)	
	µm	STEP 1 65°C	STEP 2 95°C
SU-8 2025	25	1	3
	40	1	3
	75	1	7
SU-8 2035	35	1	3
	55	1	5
	110	1	10
SU-8 2050	50	1	5
	75	1	7
	165	1	12
SU-8 2075	75	1	7
	110	1	10
	225	1	15

Table 4. Recommended post expose bake parameters

9. Development Times

Product	Thicknesses	Develop Time
	µm	min
SU-8 2025	25	4
	40	5
	75	7
SU-8 2035	35	5
	55	6
	110	10
SU-8 2050	50	6
	75	7
	165	12
SU-8 2075	75	7
	110	10
	225	12

Table 5. Recommended develop processes

10. Hard Bake

SU-8 2000 has good mechanical properties, therefore hard bakes are normally not required. For applications where the imaged resist is to be left as part of the final device, the resist may be ramp/step hard baked between 150-200°C on a hot plate or in a convection oven to further cross link the material. Bake times vary based on type of bake process and film thickness.